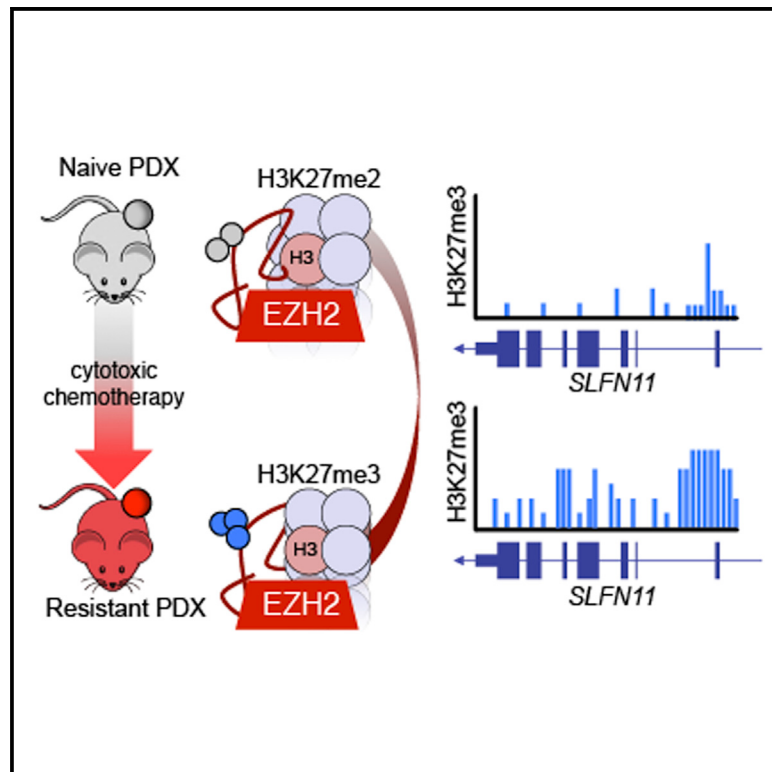


# Cancer Cell

## Chemosensitive Relapse in Small Cell Lung Cancer Proceeds through an EZH2-SLFN11 Axis

### Graphical Abstract



### Authors

Eric E. Gardner, Benjamin H. Lok,  
Valentina E. Schneeberger, ...,  
Pierre P. Masson, Charles M. Rudin,  
John T. Poirier

### Correspondence

rudinc@mskcc.org (C.M.R.),  
poirierj@mskcc.org (J.T.P.)

### In Brief

By generating paired chemonaive and chemoresistant small cell lung cancer (SCLC) patient-derived xenograft models, Gardner et al. find that EZH2 promotes chemoresistance by epigenetically silencing *SLFN11*. EZH2 inhibition prevents acquisition of chemoresistance and improves chemotherapeutic efficacy in SCLC.

### Highlights

- EZH2 drives acquired resistance to chemotherapy in small cell lung cancer (SCLC)
- DNA damage induces genome-wide EZH2 activity and H3K27me3 deposition in SCLC
- *SLFN11* is an EZH2 target gene in SCLC
- Combining an EZH2 inhibitor with standard of care controls SCLC *in vivo*

# Chemosensitive Relapse in Small Cell Lung Cancer Proceeds through an EZH2-SLFN11 Axis

Eric E. Gardner,<sup>1,2</sup> Benjamin H. Lok,<sup>2,3</sup> Valentina E. Schneeberger,<sup>2</sup> Patrice Desmeules,<sup>4</sup> Linde A. Miles,<sup>2</sup> Paige K. Arnold,<sup>5</sup> Andy Ni,<sup>6</sup> Inna Khodos,<sup>7</sup> Elisa de Stanchina,<sup>2,7</sup> Thuyen Nguyen,<sup>8</sup> Julien Sage,<sup>8</sup> John E. Campbell,<sup>9</sup> Scott Ribich,<sup>9</sup> Natasha Rekhtman,<sup>4</sup> Afshin Dowlati,<sup>10</sup> Pierre P. Mission,<sup>11</sup> Charles M. Rudin,<sup>2,12,13,\*</sup> and John T. Poirier<sup>2,13,14,\*</sup>

<sup>1</sup>Pharmacology Graduate Training Program, Department of Pharmacology and Molecular Sciences, Johns Hopkins University, Baltimore, MD, USA

<sup>2</sup>Molecular Pharmacology Program

<sup>3</sup>Department of Radiation Oncology

<sup>4</sup>Department of Pathology

<sup>5</sup>Louis V. Gerstner, Jr., Graduate School of Biomedical Sciences

<sup>6</sup>Department of Epidemiology and Biostatistics

<sup>7</sup>Anti-Tumor Assessment Core Facility

Memorial Sloan Kettering Cancer Center, New York, NY, USA

<sup>8</sup>Departments of Pediatrics and Genetics, Stanford University, Stanford, CA, USA

<sup>9</sup>Epizyme, Inc., 400 Technology Square, Cambridge, MA, USA

<sup>10</sup>Case Western Reserve University and University Hospitals Case Medical Center, Cleveland, OH, USA

<sup>11</sup>Vanderbilt Ingram Cancer Center, Vanderbilt University Medical Center, Nashville, TN, USA

<sup>12</sup>Weill Cornell Medical College, New York, NY, USA

<sup>13</sup>Department of Medicine, Memorial Sloan Kettering Cancer Center, New York, NY, USA

<sup>14</sup>Lead Contact

\*Correspondence: rudinc@mskcc.org (C.M.R.), poirierj@mskcc.org (J.T.P.)

<http://dx.doi.org/10.1016/j.ccr.2017.01.006>

## SUMMARY

Small cell lung cancer is initially highly responsive to cisplatin and etoposide but in almost every case becomes rapidly chemoresistant, leading to death within 1 year. We modeled acquired chemoresistance *in vivo* using a series of patient-derived xenografts to generate paired chemosensitive and chemoresistant cancers. Multiple chemoresistant models demonstrated suppression of *SLFN11*, a factor implicated in DNA-damage repair deficiency. *In vivo* silencing of *SLFN11* was associated with marked deposition of H3K27me3, a histone modification placed by EZH2, within the gene body of *SLFN11*, inducing local chromatin condensation and gene silencing. Inclusion of an EZH2 inhibitor with standard cytotoxic therapies prevented emergence of acquired resistance and augmented chemotherapeutic efficacy in both chemosensitive and chemoresistant models of small cell lung cancer.

## INTRODUCTION

Small cell lung cancer (SCLC) affects an estimated 270,000 individuals per year worldwide and is metastatic at the time of diagnosis in approximately two-thirds of cases (Shepherd et al., 2007; Torre et al., 2015). Metastatic SCLC is exceptionally lethal,

associated with a median survival of 9–10 months from the time of diagnosis and a 5 year survival of less than 2% (Shepherd et al., 2007). Even when detected prior to metastasis, most patients with localized disease will suffer disease recurrence and death within the first 2 years. More effective treatment approaches to SCLC are desperately needed.

## Significance

Small cell lung cancer is among the most lethal human malignancies. Typical progression of this disease is characterized by a rapid shift between initial chemoresponsive and subsequent chemoresistant states. The mechanisms responsible for acquired therapeutic resistance in small cell lung cancer have not been defined. Using patient-derived tumor xenografts to closely model clinical acquired resistance, this work: (1) defines a mechanism of chemoresistance operant across multiple, independent cancers, (2) identifies an epigenetic regulator controlling the mechanism of acquired resistance, and (3) establishes a therapeutic strategy to both prevent and treat acquired resistance *in vivo*. These observations have immediate clinical implications, describing an approach that may lead to durable and effective treatment for patients with this disease.

The standard first-line treatment for metastatic SCLC consists of a platinum doublet, cisplatin or carboplatin, generally paired with the topoisomerase II inhibitor etoposide (Kalemkerian et al., 2013). Standard approaches to recurrent SCLC include treatment with a topoisomerase I inhibitor, topotecan or irinotecan (IRI). There are no approved therapies for SCLC after progression on a second-line regimen. De novo SCLC is remarkably sensitive to first-line platinum doublet chemotherapy, with objective response rates of over 50% in patients without substantial co-morbid conditions. These impressive responses are also disappointingly transient: median progression-free survival in current trials remains less than 5 months (Belani et al., 2016). The response rates to second-line topoisomerase I inhibitor therapy are substantially lower, below 20% overall (Horita et al., 2015).

The molecular mechanisms responsible for the remarkable shift between de novo chemosensitive disease and rapidly emergent chemoresistant disease in SCLC have not been defined. Defining these mechanisms would both provide insights into the biology of SCLC and inform clinical strategies to prevent or delay therapeutic resistance. More broadly, characterizing mechanisms of acquired resistance in this cancer that undergoes a dramatic shift between chemosensitivity and chemoresistance could have implications for understanding acquired resistance to DNA-damaging cytotoxic therapy in other malignancies.

Here, we sought to discover mechanisms of acquired resistance to first-line cisplatin and etoposide (C/E) therapy in SCLC by mimicking clinical practice as closely as possible through *in vivo* treatment of a set of chemosensitive SCLC patient-derived xenograft (PDX) models. We hypothesized that an approach to detect causal alterations against a high background of tobacco carcinogen-induced passenger mutations would be to conduct a pairwise comparison of changes in individual tumor models prior to, and following, acquired chemotherapy resistance (George et al., 2015; Rudin et al., 2012).

## RESULTS

### Modeling Acquired Resistance *In Vivo*

Patients with SCLC are typically treated with a regimen of up to six cycles of chemotherapy, each cycle consisting of cisplatin on day 1 and etoposide on days 1, 2, and 3, at near maximally tolerated doses. To study mechanisms that may govern acquired chemoresistance *in vivo*, we adopted an analogous approach of repeated chemotherapy cycles in tumor-bearing animals in order to select populations of tumor cells that could effectively grow through chemotherapy (Figure 1A). We determined that we could safely administer six to eight cycles of C/E on a weekly schedule in mice. We applied this approach to ten independent PDX models of SCLC, the majority of which were derived from chemonaive patients (Table S1). We observed a spectrum of response; two out of ten models achieved complete responses, while eight out of ten showed a broad index of partial responses, ranging from 65% to 95% tumor growth inhibition, without any dose-limiting toxicity as measured by animal weights (Figures 1B and S1A–S1C). To ensure that tumors progressing through multiple cycles of chemotherapy would develop intrinsic chemoresistance, these tumors were disaggregated, re-implanted into

a second generation of mice, and selected again through multiple cycles of chemotherapy (Figure 1C). To assess the extent of acquired chemoresistance, progressing tumors re-implanted in a third generation of mice were again randomized to chemotherapy or vehicle control arms. Comparing the chemonaive with the chemoresistant state across all models, we observed a significant ( $p = 0.0008$ ) difference in the median survival time, defined as the time to reach a volumetric endpoint of 1,000 mm<sup>3</sup> (Figure 1D). Further, we observed a clear difference between the total cycles of C/E administered to naive versus resistant models ( $p = 0.026$ , Figure 1E). This was not due to a change in the time to randomization of these models (Figure 1F) or increased mitotic index as measured by Ki67 staining (Figure 1G), but rather it reflects the ability of the chemoresistant derivative tumors to grow through the selective pressure (Figures 1C and S1).

### Acquired Chemoresistance Is Not Associated with Emergence of Recurrent Mutations

We hypothesized that the development of acquired resistance to chemotherapy in these models could be caused by changes in their genetic landscapes. To investigate this, we performed whole-exome sequencing in the ten paired models. We first confirmed, by examining more than 1,000 common SNPs, that the resistant models were derived from the parental models and did not arise from cross-contamination with other cell lines, PDX, or spontaneous murine malignancies (Figure S2A). In all cases, >90% of bases could be called based on a read depth of  $\geq 15$  (Figure S2B). We observed the expected pattern of genetic alterations consistent with SCLC, including frequent alterations in TP53 and RB1 (Figure 2A). Importantly, in each case the key genetic alterations identified in the chemonaive model were maintained through acquisition of chemoresistance. We next sought to determine to what extent the total mutational burden was shared between chemonaive and chemoresistant models. A focused analysis on MSK-LX40 and MSK-LX95, two models with matched normal DNA, revealed the expected mutational pattern enriched in C > A transversions, consistent with the tobacco smoke-induced mutational signature (Alexandrov et al., 2013) (Figure 2B). The mutational signatures of these tumors were relatively stable; however, both models acquired a minor component of mutational signature 3, which has been associated with impaired double-strand break-repair by homologous recombination (Rosenthal et al., 2016). A majority of called mutations were shared, while only a minority of mutations was private to either the chemonaive or chemoresistant setting (Figure 2C). The number of private mutations was greater in the chemoresistant setting, suggesting that additional mutations were acquired during treatment. However, we were not able to identify recurrent acquired mutations across independent tumor models; no putative causal mutations of acquired resistance were found (Figure S2C), leading us to conclude that private mutations in the chemoresistant setting are passengers, not direct drivers of chemoresistance. Consistent with apparent mutational stability, we found copy-number alterations to be concordant between chemonaive and chemoresistant models and failed to identify any significant focal copy-number alterations or evidence of treatment-induced genome doubling events that could be indicative of chromosomal instability (Figure 2D). Without

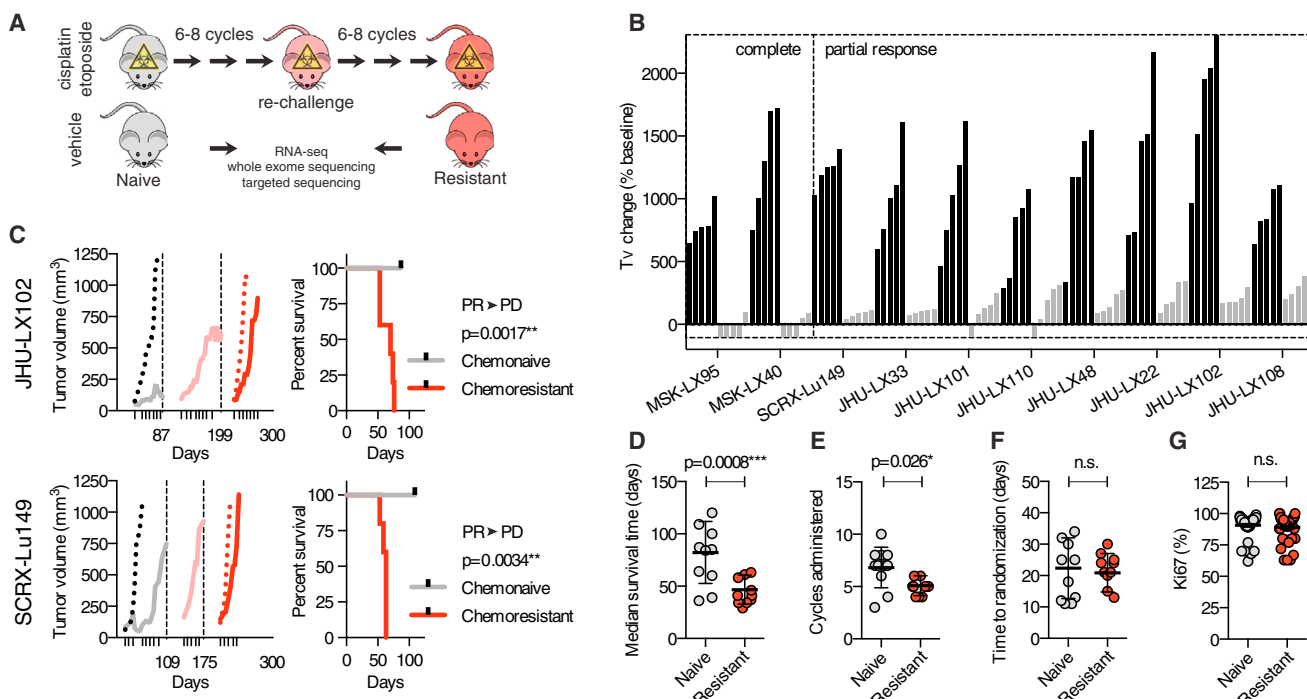


**Figure 1. Modeling Acquired Resistance C/E in SCLC**

(A) Model generation and workflow. Tumor-bearing animals were administered weekly cycles of cisplatin/etoposide (C/E) or vehicle through three sequential engraftments to generate chemoresistant models.

(B) Responses to C/E across ten SCLC PDX models. Change in tumor volume (Tv change) compared with volumes at treatment initiation (baseline). Data shown as individual bars for vehicle (black) and C/E-treated (gray) at vehicle volumetric endpoint;  $n = 5$  per group.

(C) Tumor growth kinetics of representative models JHU-LX102 and SCRXLu149. Average tumor volumes during the initial C/E challenge, vehicle (black dotted line) and treated (gray solid line). Ticks on the x axis indicate day 1 of weekly C/E cycle. Dashed vertical lines and x axis days indicate the time study treated tumors were collected and re-engrafted into secondary treated cohorts (pink solid line) and then tertiary (red; vehicle, dotted; C/E, solid line) cohorts. Survival analysis of chemonaive and chemoresistant cohorts performed using a log rank (Mantle-Cox) test. Chemosensitivity conversion status indicated above p value; PR, partial response; PD, progressive disease.

(D) Median survival time for chemonaive and chemoresistant pairs. Median survival times were calculated from survival curves of treated (naive, gray; resistant, red) cohorts. p Value is for paired t test;  $n = 10$  per group (one data point per model). Median  $\pm$  SD.

(E) Cycles of C/E administered to naive and resistant cohorts. p Value for paired t test;  $n = 10$  per group. Mean  $\pm$  SD.

(F) Time to randomization in naive and resistant cohorts. Paired t test; n.s., non-significant;  $n = 10$  per group. Mean  $\pm$  SD.

(G) Ki67 IHC-positive cells in tumors from naive and resistant cohorts. Three independent tumor cores were evaluated per model;  $n = 30$  per group. Paired t test; n.s., non-significant.

See also Figure S1 and Table S1.

clear evidence of a genetic basis for the chemoresistance phenotype, we focused subsequent analyses on potential epigenetic mechanisms of acquired chemoresistance.

### SLFN11 Suppression and TWIST1 Induction Characterize Distinct Subsets of Chemoresistant Disease

We hypothesized that there could be epigenetically driven recurrent changes in gene expression in the setting of acquired chemoresistance. To pursue this hypothesis, we performed RNA-sequencing (RNA-seq) on each of the ten paired models. Principal-component analysis suggested that gene expression patterns were remarkably consistent between chemonaive and chemoresistant settings and could easily discriminate between PDX models (Figures 3A and S3A). Due to the high degree of similarity between paired models, we hypothesized that changes in the expression of a minority of genes, as opposed to broad transcriptional changes, could drive chemoresistance. To identify

recurrently differentially expressed genes, we generated a meta p value for each gene based on the degree of differential expression in each of the individual models (Figure 3B). Schlaflen family member 11 (SLFN11), a gene that we and others have reported as being critical to sensitivity to DNA-damaging agents (Barretina et al., 2012; Lok et al., 2016; Sousa et al., 2015; Stewart et al., 2014; Tang et al., 2015; Zoppoli et al., 2012), was among the most significantly downregulated genes. Cancer-testis antigens, a family of genes that are highly sensitive to epigenetic perturbation (De Smet et al., 1999), were significantly upregulated, as well as Twist family bHLH transcription factor 1 (TWIST1), a gene described previously to play an important role in acquired resistance to a variety of agents (Fischer et al., 2015; Zheng et al., 2015). In addition to its role in therapeutic resistance, TWIST1 is a mediator of epithelial-mesenchymal transition (EMT), metastasis, and stemness (Beck et al., 2015; Schmidt et al., 2015; Yang et al., 2004, 2012). The potential mechanisms identified are mutually exclusive and together

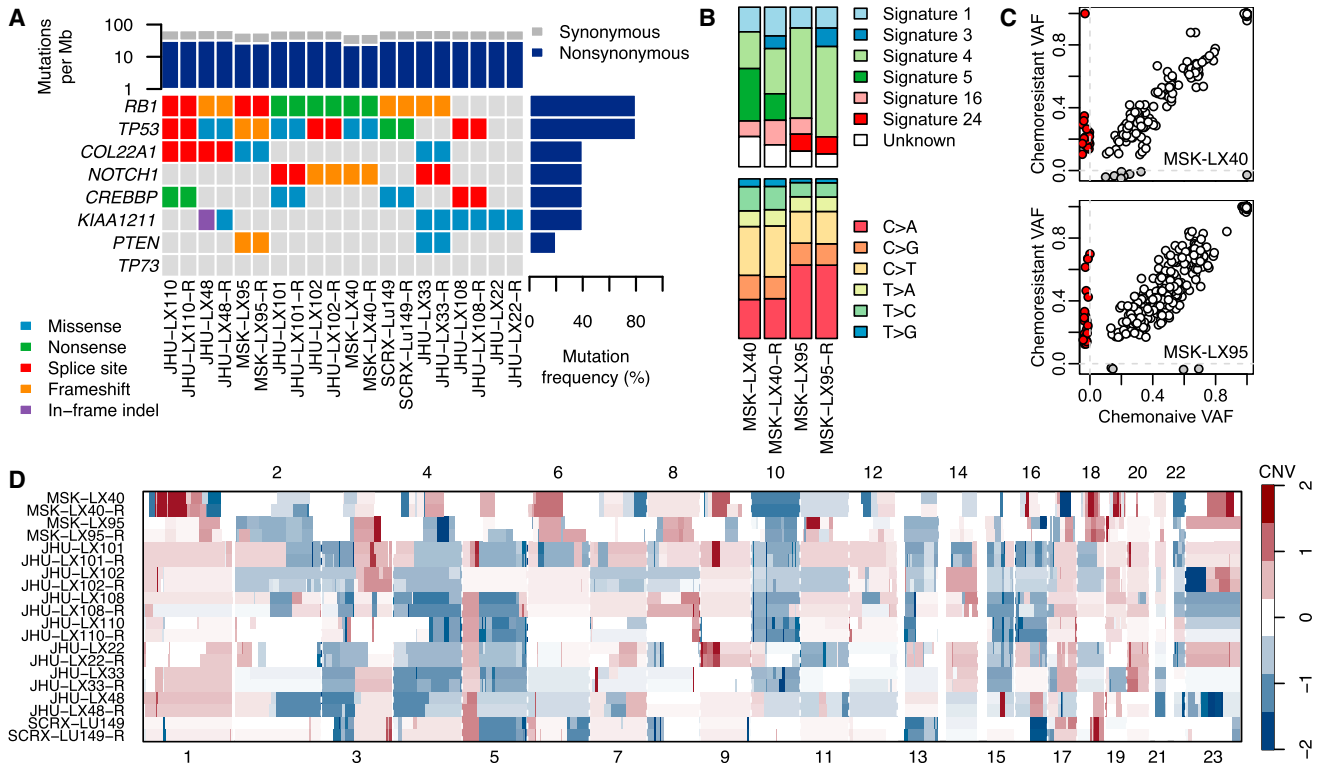


**Figure 2. Genomic Characterization of Paired Chemonaive and Chemoresistant SCLC PDX Models**

(A) Mutational analysis of paired naive and resistant PDX models by whole-exome sequencing. Shown are identifiable mutations by class among the most frequently mutated genes in primary SCLC (George et al., 2015).

(B) Analysis of mutational profiles and their associated COSMIC mutational signatures in two paired chemonaive and chemoresistant (-R) PDX models.

(C) Private versus shared mutations between paired chemonaive and chemoresistant PDX models. Colors indicate the variant allele frequencies (VAF) of the mutations, called as unique to the naive (gray) or resistant (red) tumor, with shared mutations in white.

(D) Copy-number variation (CNV) in somatic chromosomes for paired chemonaive and chemoresistant models. See also Figure S2.

are represented in seven of ten chemoresistance models (Figures 3C–3E).

We extended these results by modeling acquired resistance to C/E in murine models of SCLC (mSCLC), including two cell lines (*Rb1/Trp53* null, DKO and *Rb1/Rbl2/Trp53* null, TKO) previously generated by others (Park et al., 2011) and one chemonaive allograft directly isolated from a tumor and passaged exclusively in vivo (*Rb1/Rbl2/Trp53* null, TKO-A). Robust in vitro acquired resistance to etoposide was associated with a change in phenotype, converting from a suspension, spheroid culture to an exclusively adherent culture (Figure S3B). Using the same schedule of C/E to generate chemoresistant PDXs, we generated a chemoresistant allograft (TKO-AR). Again, the schedule of C/E was well tolerated based on animal weights and provided significant tumor growth control in the naive, but not resistant allograft ( $p = 0.0026$ , Figure S3C). Principal-component and differential gene expression analysis suggested EMT-like changes in all three models tested, with the first principal component strongly separating parental and resistant versions of the models (Figures S3D–S3F).

Given the upregulation of *TWIST1/Twist1* in both human and mouse models of SCLC upon acquired resistance, we assessed whether direct gain or loss could affect chemosensitivity. We infected the parental and resistant versions of the allograft

ex vivo with lentiviruses expressing doxycycline-inducible murine *Twist1* constructs and generated stable cell lines in culture. Notably, conditional gain of wild-type or K145E DNA-binding mutant *Twist1* (Maia et al., 2012) did not robustly change the sensitivity to etoposide, in contrast to the shift we observed ex vivo between naive and resistant allograft lines (half maximal inhibitory concentration [ $IC_{50}$ ] naive TKO-A  $\sim 0.15 \mu M$ , versus  $IC_{50}$  resistant TKO-AR  $\sim 3.0 \mu M$ ; Figure S3G). Moreover, conditional suppression of *Twist1/TWIST1* by small hairpin RNA (shRNA) could neither rescue chemosensitivity in mouse or *TWIST1*<sup>HIGH</sup> human SCLC cell lines nor influence other features of EMT observed in the resistant mSCLC cell lines, such as downregulation of E-cadherin (Figures S3G–S3I). Taken together, these results suggest that, while increases in *TWIST1* may be associated with acquired resistance to chemotherapy in SCLC, this gene does not directly promote the acquired resistance observed in our models. However, we cannot rule out the possibility that an event upstream of *TWIST1* expression may play a more direct role in acquired chemoresistance.

### SLFN11 Expression Is Decreased in Cell Lines and Clinical Samples from Previously Treated Patients

We then interrogated the role of *SLFN11* in the context of acquired chemoresistance, as it had been previously implicated

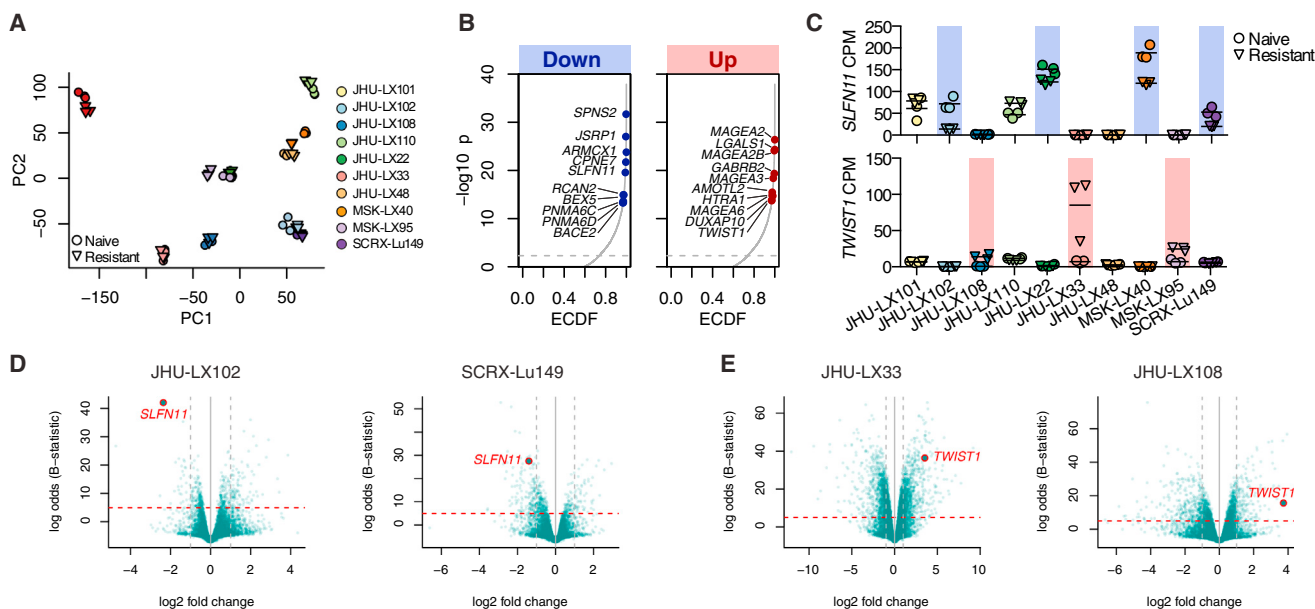


**Figure 3. Paired RNA-Seq Identifies Conserved Changes in *SLFN11* and *TWIST1***

(A) Principal-component (PC) analysis of RNA-seq data from chemonaive (circles) and chemoresistant (downward triangles) replicate samples from ten paired models.

(B) Empirical cumulative distribution function (ECDF) of combined p values of differentially down- or upregulated genes. The top ten significantly downregulated (left) or upregulated (right) genes that occur in at least three of ten models with a fold change >1.5 are indicated.

(C) Individual gene expression changes in *SLFN11* (top panel) and *TWIST1* (bottom panel) counts per million (CPM) by RNA-seq. Models with downregulated *SLFN11* and upregulated *TWIST1* are indicated by blue and red backlighting, respectively. Individual data points per tumor are shown with a horizontal line for the mean.

(D) Volcano plots demonstrating downregulation of *SLFN11* in the chemoresistant setting. Horizontal lines indicate a Beta (B)-statistic cutoff of 5; vertical lines indicate a fold change cutoff of 2.

(E) Volcano plots demonstrating upregulation of *TWIST1* in the resistant setting. Horizontal lines indicate a Best (B)-statistic cutoff of 5; vertical lines indicate a fold change cutoff of 2. See also Figure S3.

as a factor regulating DNA-damage repair (Mu et al., 2016) and was shown to correlate with responses to DNA-damaging agents in vitro (Barretina et al., 2012; Sousa et al., 2015) and in vivo (Tang et al., 2015). *SLFN11* is bimodally expressed when examined across cancer cell lines within the Cancer Cell Line Encyclopedia, as well as within SCLC in both primary tumor (Lok et al., 2016) and cell lines (Figure 4A). Many SCLC cell lines have been established and annotated with regard to their primary source (Carney et al., 1985). Cell lines generated from treated patients have lower levels of *SLFN11* expression relative to lines generated from untreated patients ( $p = 0.031$ ; Figure 4B), which also held true when comparing chemonaive with chemo-resistant PDX models ( $p = 0.003$ ; Figure 4C). We observed similar results when examining *SLFN11* protein expression by immunohistochemistry (IHC) using an H score as the comparative metric, including either all models or only models with detectable *SLFN11* at baseline (Figures 4D and 4E). In two models where chemoresistance was associated with a substantial decrease in *SLFN11* (Figure 4F), we confirmed quantitative decreases in *SLFN11* expression at both the transcript level by RNA-seq and protein level by quantitative western blotting (Figures 4G and S4A–S4C). Interestingly, an endpoint analysis of vehicle and C/E treatment groups from chemonaive and chemoresistant cohorts in one model revealed a significant decrease in *SLFN11* in progressing tumors ( $p = 0.029$ ; Figure S4D).

To assess whether *SLFN11* expression was correlated with clinical response in patients with SCLC, *SLFN11* IHC was performed on clinically annotated tumor microarrays from untreated (Vanderbilt Medical Center) and previously treated (Case Western Reserve University) SCLC patients, with H scores for each intact core determined by a pathologist blinded to sample identity (Figure 4H). Immunostaining for *SLFN11* was low to nearly absent in lung squamous cell carcinoma and adenocarcinoma in contrast to SCLC (Figure 4I). *SLFN11* expression was modestly associated with stage of disease when viewed in aggregate, with *SLFN11* greater in limited-stage versus extensive-stage patients ( $p = 0.0397$ ; Figure 4J). Consistent with a role in determining chemosensitivity, among all treated patients, *SLFN11* expression was higher in tumors from patients who responded to therapy versus those who did not ( $p = 0.0192$ ; Figure 4K). When evaluating *SLFN11* as a pretreatment predictor of response in untreated patients (Figure 4L) and as a post-treatment correlate of response (Figure 4M), we found a trend for greater *SLFN11* expression in patients categorized as treatment responsive; however, statistical significance was not reached. Notably, among untreated patients, 83% (10/12) of patients with a *SLFN11* H score >75 responded to treatment (Figure 4L); using the same threshold among previously treated patients, all six patients with an H score >75 responded to treatment (Figure 4M). However, applying a dichotomized H score of 68.8 using Youden's index (Youden, 1950) did not show a statistically significant difference

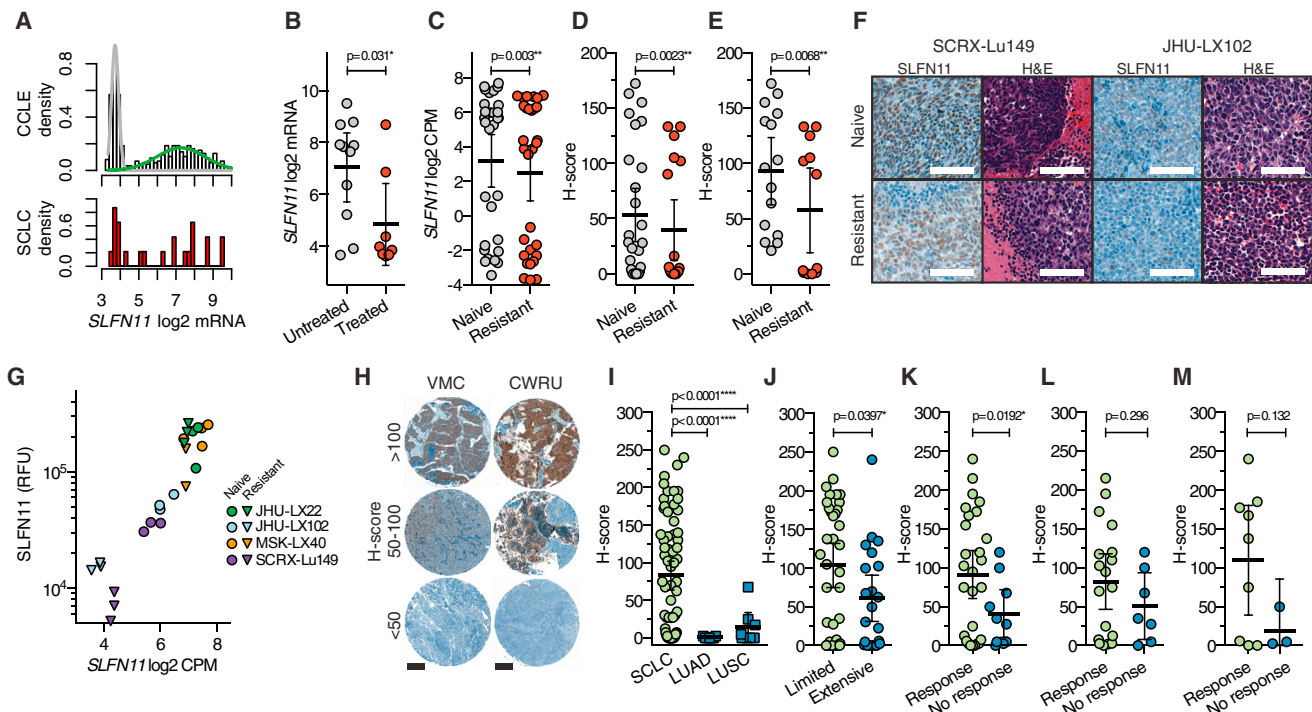


**Figure 4. SLFN11 Is Downregulated at the Transcript and Protein Level in SCLC Following Exposure to Chemotherapy**

(A) Density histograms of *SLFN11* gene expression across the Cancer Cell Line Encyclopedia (CCLE) dataset and SCLC cell lines within CCLE. Cell lines in CCLE are shown as density distributions of those that express little to no *SLFN11* (gray) versus the broad distribution of *SLFN11* levels in other lines (green). SCLC cell lines are shown in red (lower panel).

(B) Comparison of *SLFN11* expression in SCLC cell lines derived from untreated or treated patients;  $p = 0.031$ , Fisher's exact test. Treatment history is available in Polley et al. (2016). Mean  $\pm$  SD.

(C) *SLFN11* gene expression in all chemonaive and chemoresistant PDX models. Three replicates per model, per condition are plotted;  $n = 30$  per group. Mean  $\pm$  SD.  $p$  Value for paired Student's t test.

(D) *SLFN11* IHC scoring metric (H score) compared between all chemonaive and chemoresistant PDX models. Three independent core samples per model, per condition;  $n = 30$  per group. Mean  $\pm$  SD.  $p$  Value from Mann-Whitney test.

(E) H score comparison including only models with detectable *SLFN11* by IHC (IHC-positivity  $\geq 1+$  and one core with H score  $>20$ ; 5/10 PDX models included).  $p$  Value from Mann-Whitney test. Mean  $\pm$  SD.

(F) Representative *SLFN11* IHC and H&E sections from two models (SCRX-Lu149 and JHU-LX102) in the chemonaive and chemoresistant cohorts. Scale bars, 100  $\mu$ m.

(G) Concordance between *SLFN11* gene expression by RNA-seq and *SLFN11* protein expression by quantitative western blot. RFU, relative fluorescence units.

(H) Representative IHC staining for *SLFN11* in clinically annotated SCLC TMAs. VMC, Vanderbilt Medical Center; CWRU, Case Western Reserve University. Scale bars, 200  $\mu$ m, for entire 1 mm cores.

(I) *SLFN11* expression by IHC in SCLC, lung adenocarcinoma (LUAD), and squamous cell carcinoma (LUSC). Sixty out of 215 untreated VMC and 12/22 treated CWRU cores were evaluable for comparison. Seven LUAD and seven LUSC samples were evaluated.  $p$  Values from unpaired two-tailed t tests. Mean  $\pm$  95% confidence interval (CI).

(J) Comparison of *SLFN11* H score by stage of patient from pooled analysis of VMC and CWRU TMAs.  $p$  Values from unpaired t tests. Mean  $\pm$  95% CI.

(K) Comparison of *SLFN11* H score by response of patients from both cohorts. Responses include complete or partial response, where no response includes progressive or stable disease.  $p$  Values from unpaired t tests. Mean  $\pm$  95% CI.

(L) Comparison of *SLFN11* H score by response of patients from the untreated cohort.  $p$  Values from unpaired t tests. Mean  $\pm$  95% CI.

(M) Comparison of *SLFN11* H score by response of patients from the previously treated cohort.  $p$  Values from unpaired t tests.

See also Figure S4. Mean  $\pm$  95% CI.

in overall survival ( $p = 0.884$ , log rank test; Figure S4E). Taken together, these data suggest that high *SLFN11* expression in SCLC confers greater sensitivity to chemotherapy but does not confer an overall survival benefit in this clinical cohort.

#### EZH2 Inhibition Restores *SLFN11* Expression and Chemosensitivity In Vitro

A recent report suggested that *SLFN11* expression is partly regulated by an epigenetic silencing mechanism reversed by

broad DNA methylation inhibitors such as 5-azacitidine (5-Aza) (Nogales et al., 2016). We chose to examine whether EZH2 (enhancer of zeste homology 2) could have a role in silencing *SLFN11* in SCLC for several reasons: (1) there is evidence for an EZH2 binding site upstream of the first exon of *SLFN11* from cell line data reported by the ENCODE project (Gerstein et al., 2012; Wang et al., 2013), (2) we have shown EZH2 expression levels to be higher in SCLC than in any of the tumor types included in TCGA (Poirier et al., 2015), and (3) others have shown

that PRC2 target gene repression correlates with shorter survival in primary SCLC (Sato et al., 2013). Overall, these lines of evidence prompted us to examine whether chemical inhibitors targeting DNA or histone methyltransferase enzymes could play a role in regulating *SLFN11* expression.

Using short-term ex vivo culture, we exposed naive and resistant versions of select PDX models to either 5-Aza or the EZH2 inhibitor EPZ011989 (abbreviated EPZ). After 7 days of continuous daily exposure, we noted striking increases in *SLFN11* expression in the EPZ-treated cells versus DMSO- or 5-Aza-treated cells, suggesting that *SLFN11* expression may be regulated at the level of histone methylation, rather than DNA methylation, in SCLC (Figure 5A). Moreover, treatment with EPZ, but not 5-Aza, effectively restored ex vivo etoposide sensitivity of the chemoresistant model to that of the chemonaive model, where ex vivo resistance was most pronounced for topoisomerase inhibitors and less for cisplatin (Figures 5B and 5C). We next interrogated the kinetics of *SLFN11* re-expression in the SCLC cell line NCI-H82, which was derived from a previously treated patient and shows minimal expression of the *SLFN11* protein. We monitored the re-expression of *SLFN11* over a 21 day period in suspension culture, during which time cells were treated daily with 1  $\mu$ M EPZ for 10 days and then cultured in fresh medium without compound for an additional 10 days. We noted striking re-expression of *SLFN11* after ~7–10 days of drug exposure, with concomitant suppression of H3K27me2/3, consistent with on-target inhibition of EZH2 (Figure 5D). Re-expression of *SLFN11* was dose-dependent and stable under acute DNA damage (Figure S5A). This re-expression was sustained even as global H3K27me2/3 levels returned to baseline levels during a 10 day washout period (Figure 5D). In 7 day treatment assays, we noted a dramatic increase in *SLFN11* protein expression in cell lines with little to no detectable *SLFN11* (Figure 5E). This was in contrast to cell lines with high de novo expression of *SLFN11*, in which no further increase above baseline was observed. The extent to which *SLFN11* protein levels were increased by EPZ was strongly correlated to an increase in topotecan sensitivity across all cell lines tested (Pearson's  $r = 0.916$ ; Figures 5F and S5B). *SLFN11* protein re-expression by EPZ was suppressible with shRNAs targeting *SLFN11* (Figures S5C and S5D). *SLFN11* expression could also be induced with GSK126, a chemically distinct EZH2 inhibitor, although EPZ showed greater capacity for *SLFN11* re-expression when compared with GSK126, which had comparatively less robust H3K27me3 suppression in our experience (McCabe et al., 2012).

A shift in global repressive histone methylation may have pleiotropic effects on gene expression that manifest in a cell-line-specific manner (Jadhav et al., 2016). To directly address whether re-expression of *SLFN11* was sufficient to sensitize SCLC cell lines with low levels of *SLFN11* to DNA-damaging agents, such as topotecan, we used a doxycycline-inducible expression vector to express *SLFN11* in NCI-H82 and NCI-H446. Both of these cell lines were derived from previously treated patients and are highly resistant to etoposide. Exogenous expression of *SLFN11* was capable of sensitizing these cell lines to topotecan relative to non-induced or empty vector controls (Figure 5G), although this effect was less pronounced than that of the EPZ-mediated sensitization (Figure 5C). Consistent with this observation, shRNA-mediated suppression of *SLFN11* in NCI-H526, a cell line with high baseline *SLFN11* expression, modestly

decreased the sensitivity of this line to topotecan, although we note that complete suppression of *SLFN11* was not possible even with a potent shRNA (Figure S5E). Remarkably, while EPZ treatment shifted the sensitivity of NCI-H82 cells to topotecan by approximately one log, this was reversed by concurrent shRNA suppression of *SLFN11* (Figures 5H and 5I). While we did not note changes in markers of acute DNA-damage response ( $\gamma$ H2A.X), we found that EPZ-treated cells showed increased markers of programmed cell death (cleaved-PARP) upon acute topotecan exposure that were reduced when suppressing *SLFN11* by shRNA (Figure 5J). Taken together, these data strongly implicate *SLFN11* as a determining factor in sensitivity to DNA-damaging agents in SCLC.

### EZH2 Silences *SLFN11* Expression in SCLC

To further define the mechanistic relationship between EZH2 and *SLFN11* expression, we sought to explore the effects of EZH2 inhibition on local chromatin structure in the vicinity of the *SLFN11* locus. We examined the efficacy of EPZ in four PDX models at two dose schedules over a treatment period of 3 weeks (Table S2). This schedule slowed tumor growth modestly in three of four models tested (Figure S6A), and EPZ was well tolerated in animals based on weight measurements when administered at 250 mg/kg orally, twice a day (PO bid) (Figure S6B). This analysis included a chemorefractory model, JHU-LX44, that was omitted from the analysis of chemosensitive models (Figures S6C). Our ability to observe single-agent efficacy in vivo may have been limited by the duration we were able to treat animals relative to the time required to remodel the epigenome, which is thought to require weeks to months (LaFave et al., 2015). We further assessed the contribution of time-dependence for efficacy in vivo by re-engrafting equivalent viable cell numbers from tumors that had previously been treated for 21 days with or without EPZ, and then re-treating tumors with vehicle or a secondary round of EPZ as soon as tumors became palpable (Figure S6D). These results suggest that prolonged exposure of SCLC tumors to EZH2 inhibition may have a greater effect on decreasing proliferative capacity; however, continuous treatment led to weight loss that approached protocol limits.

To demonstrate the ability of EPZ to modulate the SCLC chemoresistant epigenome, we performed chromatin immunoprecipitation followed by sequencing (ChIP-seq) from flash frozen tissue collected from chemonaive or chemoresistant SCRXLu149 tumors treated for 21 days with vehicle or EPZ. ChIP-seq was performed on three targets: EZH2, H3K27me3, and H3K27Ac (Figure 6A). While total EZH2 levels were not significantly altered in any condition, we observed increased global H3K27me3 in the chemoresistant setting that could be abolished by EPZ, as well as decreased global H3K27Ac in the chemoresistant setting that could be rescued by EPZ. Global H3K27Ac levels were increased by EPZ in both the chemonaive and chemoresistant settings with concomitant loss of H3K27me3. The global reduction of H3K27Ac in the chemoresistant setting prompted us to explore differential intensities within genomic regions termed super-enhancers (Loven et al., 2013; Pott and Lieb, 2015), thought to be critical for SCLC proliferation (Christensen et al., 2014; Lin et al., 2012). We observed differential signal intensities in such regions, consistent with global loss of H3K27Ac in the chemoresistant setting, which could be restored

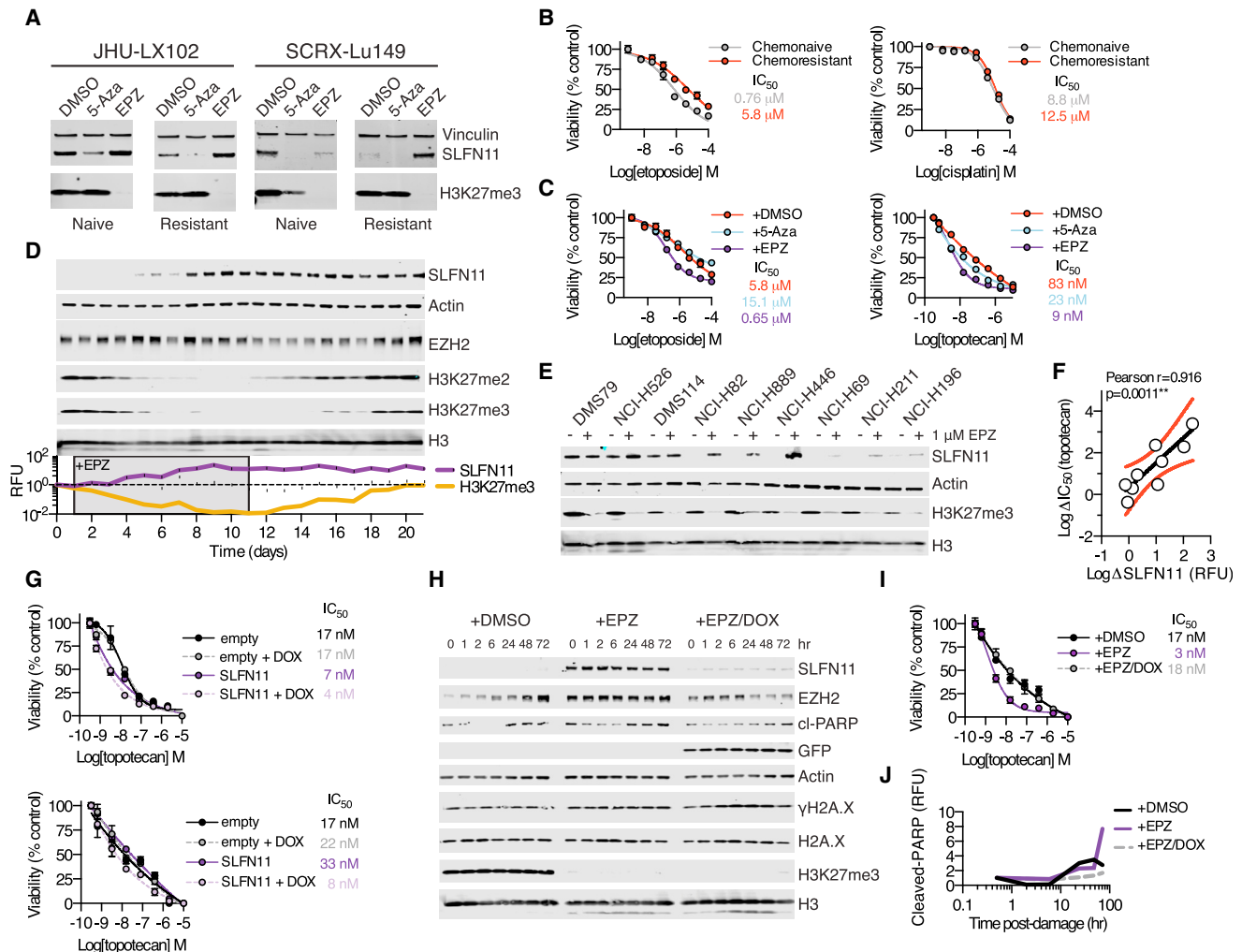


**Figure 5. Chemical EZH2 Inhibition Rescues SLFN11 Expression and Sensitizes SCLC to DNA Damage**

- (A) Chemonaive and chemoresistant PDX models JHU-LX102 and SCRXLu149 cultured ex vivo and treated for 7 days with 1  $\mu$ M of 5-azacitidine (5-Aza) or EPZ daily and then assayed by western blot.
- (B) Viability of chemonaive and chemoresistant JHU-LX102 upon treatment with etoposide and cisplatin for 72 hr.  $n = 3$ /data point; mean viability  $\pm$  SEM.
- (C) Viability for etoposide (left)- and topotecan (right)-treated chemoresistant JHU-LX102 with or without co-treatment with 5-Aza or EPZ. Cells were treated as in (A) for 7 days before re-plating and exposure to either etoposide or topotecan for 72 hr as above.  $n = 3$ /data point; mean viability  $\pm$  SEM.
- (D) NCI-H82 cells treated daily for 10 days with 1  $\mu$ M EPZ then washed and released into fresh medium for 10 days. The medium was changed every other day. Samples were collected every day for 21 days and assayed by western blot. Relative fluorescence units (RFUs) for SLFN11 and H3K27me3 are shown.
- (E) SCLC cell lines cultured with 1  $\mu$ M EPZ for 7 days, refreshing the compound every day and the medium every other day prior to collection of samples and western blot.
- (F) Correlation of SLFN11 expression upon chemical EZH2 inhibition to sensitivity to topotecan. Pearson's correlation  $r = 0.916$ . Red lines represent 95% confidence intervals.
- (G) Conditional re-expression of SLFN11 and topotecan sensitivity in NCI-H82 (top) and NCI-H446 (bottom). Cells were transduced and expression was induced with doxycycline (DOX) at 1  $\mu$ g/mL added every other day for 4 days before re-plating for 72 hr with topotecan.  $n = 3$ /data point; mean viability  $\pm$  SEM.
- (H) NCI-H82 cells were transduced with DOX-inducible shRNA against SLFN11 and exposed to DMSO, 1  $\mu$ M EPZ, or EPZ/DOX for 7 days before exposure to 1  $\mu$ M topotecan for 1 hr. Cells were then released into fresh medium and collected at the given time points for western blot. cl, cleaved.
- (I) Effect of topotecan on NCI-H82 cells expressing shRNA against SLFN11 after 7 days of treatment with DMSO, 1  $\mu$ M EPZ, or 1  $\mu$ M EPZ and EPZ/DOX. Following treatment, cells were exposed to the indicated amounts of topotecan for 72 hr.  $n = 3$ /data point; mean viability  $\pm$  SEM.
- (J) Cleaved-PARP RFUs from (H). RFU normalized to un-damaged controls following 7 days of treatment (0 hr for DMSO, EPZ, or EPZ/DOX). See also Figure S5.

with EPZ. However, selective loss or rescue of discrete super-enhancer regions was not observed (Figure 6B).

Focusing specifically on the SLFN11 locus, ChIP-seq data demonstrate focally concentrated EZH2 and H3K27me3 in the immediate vicinity of the transcription start site (TSS) in

vehicle-treated tumors, with spreading of H3K27me3 across the gene body in the context of acquired chemoresistance (Figure 6C). Coordinate with the increase in H3K27me3 across the gene body in the chemoresistant versions, there is almost complete loss of H3K27Ac, a mark associated with transcriptionally

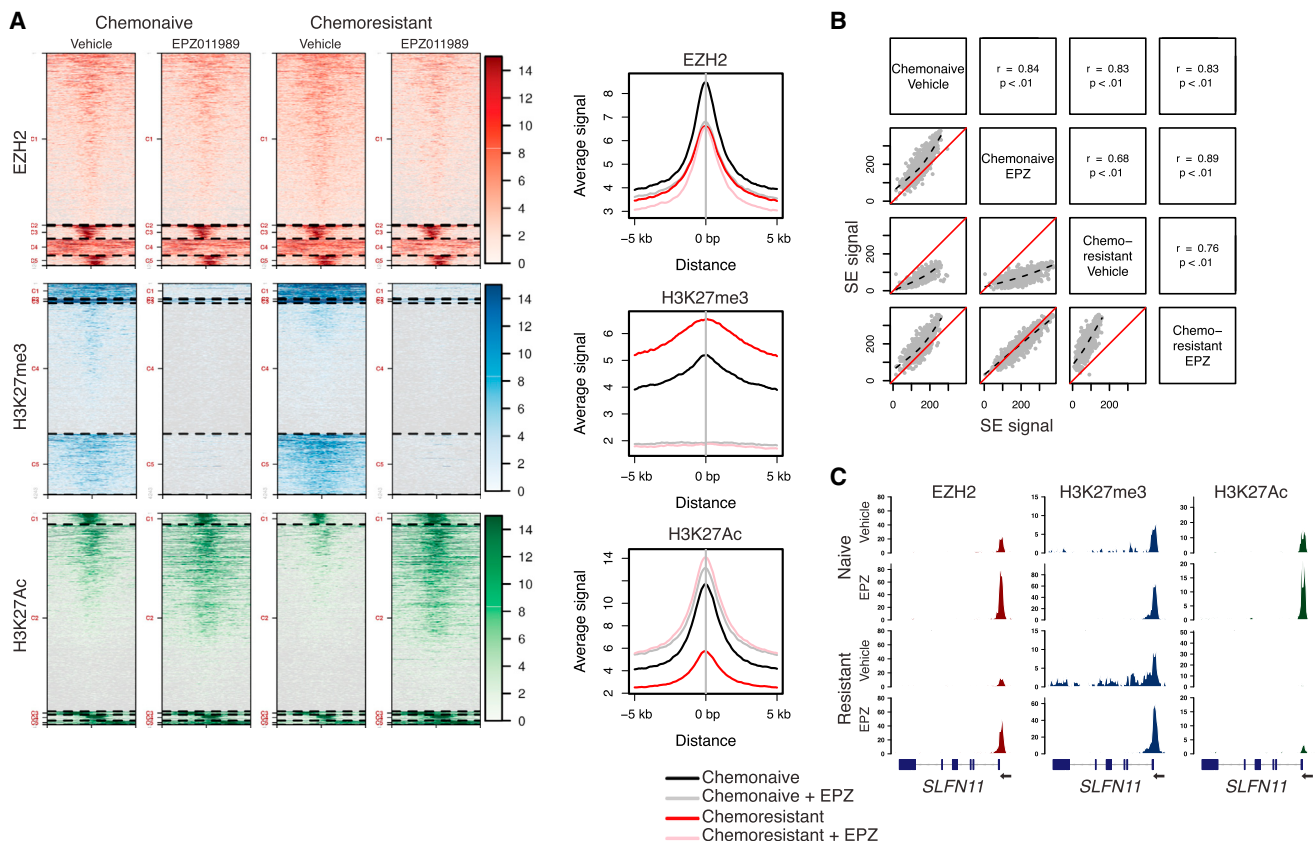


**Figure 6. Epigenetic Changes Acquired in Chemoresistance Are Reversible with Chemical EZH2 Inhibition In Vivo**

(A) Cluster analysis of ChIP-seq results from four SCRX-Lu149 tumor groups: chemonaive or chemoresistant treated with either vehicle or 250 mg/kg EPZ PO bid for 21 days. Chromatin was pooled from three independent tumor samples per arm prior to immunoprecipitation.

(B) Scatterplots of super-enhancer signal intensity. Spearman's rank correlation coefficient and p value are calculated for each comparison. Dotted black lines are locally weighted polynomial regressions. Solid red lines indicate unity.

(C) *SLFN11* ChIP-seq gene tracks for the indicated sample treatment arms. The limits of the y axes are scaled to *Drosophila* spike-in for each sample for peak height comparisons. The *SLFN11* gene model is oriented right-to-left along the x axis as indicated. See also Figure S6 and Table S2.

active chromatin, at the TSS of *SLFN11*, which we confirmed by ChIP-qPCR ( $p < 0.0001$ ; Figure S6E). Interestingly, EPZ treatment increased the density of EZH2 bound near the *SLFN11* TSS and largely erased H3K27me3 throughout the gene body of *SLFN11*. Levels of H3K27me3 near the TSS remained largely unchanged. We further confirmed gene body erasure of H3K27me3 within exons 2–7 of *SLFN11* by exon-by-exon ChIP-qPCR (Figure S6F). EPZ treatment also resulted in an increase in levels of H3K27Ac near the *SLFN11* TSS and throughout the gene body. These data suggest that re-expression of this EZH2 target gene via chemical inhibition may also require cooperative histone modifications to promote gene expression. While we observed rescue of *SLFN11* in PDX models that downregulated the gene upon acquiring resistance to C/E, expression was not rescued in models that expressed low to undetectable levels of *SLFN11* at baseline (Figure S6G).

#### Pharmacologic EZH2 Inhibition Prevents Emergence of Chemoresistance and Augments Chemosensitivity In Vivo

The downregulation of *SLFN11* in acquired chemoresistance and its apparent regulation by EZH2 suggest a model in which

EZH2 is induced by cytotoxic chemotherapy, resulting in deposition of repressive chromatin marks in the *SLFN11* gene body, decreasing expression and promoting chemoresistance. To test this hypothesis and evaluate time-dependent changes in EZH2 activity, we performed DNA-damage time-course experiments in NCI-H446, following exposure to topotecan in the presence or absence of EPZ. Over the course of 48 hr following DNA damage, we noted a progressive increase in EZH2, as well as H3K27me3, which was suppressed by EPZ (Figure 7A). Further, we could demonstrate that the effect on H3K27me3 was a function of EZH2, as shRNA suppression of EZH2 during a similar DNA-damage time course abolished any increase in H3K27me3 and the accompanying loss of H3K27me2 (Figure 7B). These data support a global methylation event where di-methylated H3K27 is converted to the tri-methylated state. The effect of DNA damage increasing global H3K27me3 levels was not cell-line specific (Figure S7A), demonstrated dose dependence (Figure S7B), and was more pronounced for topotecan when compared with either cisplatin or etoposide on an equimolar basis (Figure S7C). These shifts in EZH2 activity and resultant H3K27me3 were also observed in vivo, using a single dose-chase approach in tumor-bearing animals treated with

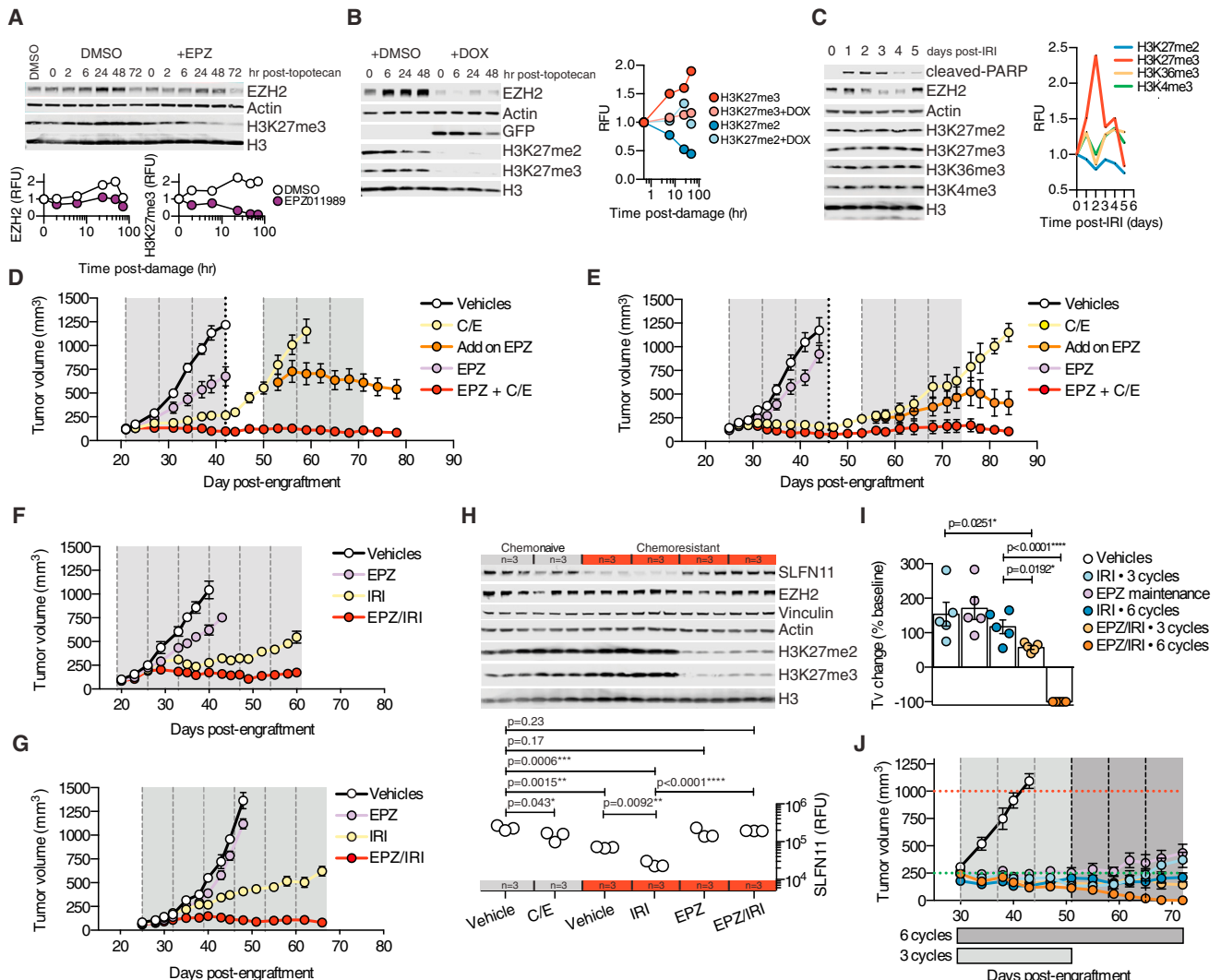


**Figure 7. EZH2 Is an Actionable Target in Combination with Standard of Care in SLFN11<sup>HIGH</sup> SCLC**

- (A) NCI-H446 cells exposed to 1  $\mu$ M topotecan for 1 hr  $\pm$  1  $\mu$ M EPZ. Cells were then washed and collected at time points for western blot. Quantified EZH2 and H3K27me3 fluorescence units (RFU) over time.
- (B) NCI-H446 cells transduced with EZH2 shRNA treated  $\pm$  1  $\mu$ g/mL doxycycline (DOX) for 48 hr before adding 1  $\mu$ M topotecan, as in (A). On the right, quantified H3K27me3 and H3K27me2 (RFU) over time.
- (C) Size-matched chemonaive JHU-LX102 tumor-bearing mice ( $\sim$ 400 mm<sup>3</sup>) treated intraperitoneally with 100 mg/kg IRI and tumors collected at the indicated time points post-dose for western blot.
- (D) SLFN11<sup>HIGH</sup> chemonaive JHU-LX102 tumor volume responses. Dashed vertical lines indicate day 1 of a weekly C/E cycle. The dotted line indicates five of the ten animals within the C/E group now randomized to receive EPZ with three additional cycles of C/E. Gray areas indicate the dosing periods for EPZ (250 mg/kg PO bid). n = 5 per arm (n = 10 in C/E arm through three cycles, before adding on EPZ). Tumor volume mean  $\pm$  SEM.
- (E) Results for chemonaive SCRXLu149 treated as in (D). Tumor volume mean  $\pm$  SEM.
- (F) Chemoresistant JHU-LX102 tumor volume responses. Dashed vertical lines indicate day 1 of a cycle. Six weekly cycles of IRI  $\pm$  EPZ or single-agent EPZ. n = 5 per arm. Tumor volume mean  $\pm$  SEM.
- (G) Results for mice engrafted with chemoresistant SCRXLu149 as in (F). n = 5 per arm. Tumor volume mean  $\pm$  SEM.
- (H) Western blot analysis for SLFN11 suppression and rescue in chemonaive (gray bar; n = 6) or chemoresistant (red bar; n = 12) JHU-LX102 treated as labeled and collected at day 21. Tumors were size matched ( $\sim$ 400 mm<sup>3</sup>) per cohort. SLFN11 (RFU) quantified below; n = 3/arm. Three cycles of each indicated treatment arm were administered before collecting tumors. Values from paired t tests.
- (I) Change in tumor volume (Tv) from volumes at treatment initiation (baseline) in chemonaive JHU-LX102 treated with three or six weekly cycles of 100 mg/kg IRI and/or EPZ. Comparison at 6 weeks post-treatment (day 72). n = 5/arm. Dots indicate Tv change of individual tumors and bars indicate average  $\pm$  SEM. p Values from paired t tests.
- (J) Chemonaive JHU-LX102 response (n = 5 per arm) to three or six weekly cycles of 100 mg/kg IRI and/or EPZ. Horizontal dashed lines indicate starting (green) and ending (red) tumor volumes. Group duration along the x axis. Vertical dashed lines indicate a weekly cycle of IRI. Tumor volume mean  $\pm$  SEM.

See also Figure S7 and Table S3.

IRI and quantitatively evaluating time-dependent changes in several H3 methyl marks, demonstrating specificity for the induction of H3K27me3, with contemporaneous decreases in H3K27me2 ([Figure 7C](#)).

These data support the hypothesis that EZH2 activity is an important determinant of acquired chemotherapy resistance in SCLC. To examine the efficacy of EPZ with cytotoxic regimens *in vivo*, we chose two clinically translatable scenarios: (1) combining EPZ with standard of care in the first-line setting for SLFN11 expressing (SLFN11<sup>HIGH</sup>) chemonaive models and (2) combining EPZ with a standard second-line agent in the chemoresistant setting, in which the silencing of *SLFN11* has been established. Addition of EPZ to six cycles of C/E strongly enhanced disease control in the chemonaive setting in both JHU-LX102 and SCR-X-Lu149 relative to either EPZ or C/E alone without increasing animal weight loss ([Figures 7D, 7E, S7D, and S7E](#)). To examine the benefit of EZH2 inhibition in tumors actively progressing on C/E, after three cycles we randomized five of ten animals in the C/E arm to receive EPZ in combination with three additional cycles of C/E. Remarkably, the addition of EPZ potently induced tumor regression relative to C/E alone during the remaining three cycles, supporting a role for EZH2 in promoting chemoresistance ([Figures 7D and 7E](#)).

We next assessed the efficacy of IRI, a topoisomerase I poison administered in the setting of relapsed SCLC, with or without EPZ, in chemoresistant JHU-LX102 and SCR-X-Lu149. Importantly, we observed strong cross-resistance to IRI, but not ionizing radiation, in the chemoresistant setting, further supporting the mechanism of acquired resistance operant in these models had specificity to the selection agents used (cisplatin and/or etoposide) ([Figures S7F and S7G](#)). The addition of EPZ to IRI in the chemoresistant setting resulted in potent combinatorial activity that could control disease to a greater extent than either agent alone through six weekly cycles of treatment without increasing animal weight loss ([Figures 7F, 7G, S7H, and S7I](#)).

To further assess active repression and de-repression of *SLFN11* *in vivo*, we used chemonaive and chemoresistant versions of JHU-LX102, randomizing size-matched tumors (~400 mm<sup>3</sup>) to three cycles of chemotherapy ± EPZ. Strikingly, we noted quantitative suppression of *SLFN11* in tumors after as few as three cycles of C/E in the chemonaive setting, with further suppression after three cycles of IRI in the chemoresistant setting ([Figure 7H](#)). Critically, EZH2 inhibition could rescue *SLFN11* to baseline levels in the chemoresistant setting, even in the presence of concurrent chemotherapy (chemonaive vehicle versus chemoresistant EPZ/IRI).

In combining EPZ with IRI in the chemonaive setting, we could completely ablate hind flank tumors through six cycles of combination (complete response in five out of five animals; [Figures 7I and 7J](#)). Moreover, the activity of the combination was greater, even when administered for a shorter duration of time (three cycles), than the equivalent schedule of IRI administered for six cycles. However, we did not observe additional benefit when initiating adjuvant EPZ as a single agent at the point of maximal consolidative effect of single-agent IRI (post cycle 3), as this was inferior to three additional cycles of IRI at the point of comparison. When comparing the responses of a *SLFN11*<sup>HIGH</sup> with a *SLFN11*<sup>LOW</sup> model, both chemonaive models displayed sensitivity to IRI, but only in the *SLFN11*<sup>HIGH</sup>

model is the combined activity of EPZ and IRI strikingly different ([Figures S7J and S7K](#)). Moreover, while all *SLFN11*<sup>HIGH</sup> JHU-LX102 tumors in the combination arm were ablated after six cycles, tumors eventually recurred yet still maintained comparable sensitivity to the combination ([Figure S7K](#)). Recurrent tumors appeared similar to untreated tumors, not displaying differentiation away from their proliferative, neuroendocrine features ([Figures S7L](#)). Body weight and repeat blood chemistry monitoring during 2 weeks of treatment revealed no significant toxicity of the combination compared with single agents ([Figure S7M and Table S3](#)). Further, gross necropsy also suggested no apparent major organ toxicities ([Figure S7N](#)). Taken together, combining a clinical stage EZH2 inhibitor with a topoisomerase I poison is well tolerated and highly effective in *SLFN11*-expressing SCLC.

## DISCUSSION

SCLC has been singled out by the US National Cancer Institute as a designated “recalcitrant” cancer based on incidence rate, exceptionally high lethality, and the lack of substantial therapeutic progress made over several decades. By mimicking the clinical experience of repeated cycles of C/E exposure in PDXs, we have generated a set of paired models representing initial chemosensitive and subsequent chemoresistant disease. We used these models to define two mutually exclusive mechanistic classes of acquired resistance, including an EMT shift associated with *TWIST1* upregulation and epigenetically mediated suppression of *SLFN11*. Finally, we have identified a therapeutically tractable vulnerability in SCLC: dependence on the activity of EZH2 for the development of acquired chemoresistance.

We found that consistent gene expression and epigenetic changes, not mutations, are associated with acquired chemoresistance across independent SCLC models and indeed are reflected in primary human tumor samples. In a set of ten PDX models, *TWIST1* induction was observed in three; this pathway was additionally reflected in multiple murine models of SCLC. While initial data point to *TWIST1* as a biomarker rather than a driver of resistance per se, further exploration of therapeutic vulnerabilities associated with an EMT signature in this set of tumors is warranted. In four of the ten PDX models, acquired resistance was associated with specific suppression of *SLFN11*. Most notably, our data point to *SLFN11* suppression as a primary contributor to acquired chemotherapy resistance in SCLC, one that can be prevented and/or actively remodeled through targeting EZH2.

We have demonstrated here that *SLFN11* suppression during selection for acquired resistance in SCLC is associated with a global increase in H3K27me3 with modest reductions in global H3K27Ac, and that *SLFN11* gene expression can be restored and/or maintained by pharmacological inhibition of EZH2, even in the presence of DNA-damaging agents. While we have shown that *SLFN11* is both necessary and sufficient for sensitivity to DNA-damaging agents in SCLC, we recognize that EZH2 inhibition alters expression of many genes. We anticipate that factors beyond *SLFN11* will be identified that contribute to the ability of EZH2 inhibition to restore chemosensitivity in SCLC. Defining the relative contributions of *SLFN11*

versus other EZH2-modified factors remains an area for future investigation.

Several potent and selective EZH2 inhibitors are now in different stages of clinical development, including phase II (Epizyme) and phase I (Constellation, GSK) trials in multiple solid tumor and hematological indications. Epizyme recently updated the phase I experience and ongoing phase II experience for their lead inhibitor tazemetostat (EPZ-6438) (Ribrag et al., 2016; Morschhauser et al., 2016), which is a closely related structural homolog of the tool compound inhibitor EPZ011989 described in this paper (Fillmore et al., 2015). The safety profile of tazemetostat in 82 patients with non-Hodgkin lymphoma on the ongoing phase II study was favorable, with the most frequent treatment-related adverse events being grade 1 or 2 nausea and asthenia. Myelosuppression was observed infrequently, with only 11% and 6% of patients experiencing grade  $\geq 3$  thrombocytopenia and grade  $\geq 3$  neutropenia, respectively, suggesting that tazemetostat may be safely combined with cytotoxic chemotherapy in SCLC. Importantly, the work presented here suggests that targeted EZH2 inhibitors should be anticipated to have minimal single-agent activity in SCLC, and that evaluation of relevant combination therapies should be considered early in clinical development of these agents in SCLC. Clinical trials testing the therapeutic strategies defined here are now being designed with these considerations in mind.

## EXPERIMENTAL PROCEDURES

### PDXs

All animal experiments were approved by the Memorial Sloan Kettering Cancer Center (MSKCC) Animal Care and Use Committee. Primary tumors and whole-blood samples collected for generation of PDX models were obtained with informed consent from patients under protocols approved by the MSKCC and JHMI institutional review boards. Subcutaneous flank tumors were generated as described previously (Daniel et al., 2009). A list of PDX model details can be found in Table S1.

### DNA/RNA Sequence Alignment

Raw reads were aligned to custom human/mouse hybrid references as described previously (Schneeberger et al., 2016). In brief, hybrid indexes were generated using a FASTA file consisting of all human GRCh38 and mouse GRCm38.p3 reference contigs and, in the case of RNA-seq, assisted by the human GENCODE gene set release 20 transcript model. Downstream analysis was performed with reads mapping to human reference contigs.

### Statistics

Sample sizes per *in vivo* groups were at a minimum of five per condition, unless specified within the text for purposes of endpoint analysis. Power calculations and sample size estimates were not performed. Student's *t* tests, one-way ANOVA, Pearson's correlation, and log rank tests were performed using GraphPad Prism version 6.00 for Mac GraphPad Software, [www.graphpad.com](http://www.graphpad.com). For *in vitro/ex vivo* dose-response curves, best fit IC<sub>50</sub> values are reported from normalized datasets using the equation, log (inhibitor) versus response – variable slope, with an ordinary fitting method. At least three data points per dose were used, with experiments being performed at least twice. Error bars for SD or SEM are shown. Where indicated in the figures, degrees of *p* value significance are as follows: \**p* < 0.05, \*\**p* < 0.005, \*\*\**p* < 0.0005, and \*\*\*\**p* < 0.0001.

### ACCESSION NUMBERS

All raw data resulting from RNA-seq, whole-exome sequencing, and targeted sequencing is available from the database of Genotypes and Phenotypes (dbGaP) under accession number phs001249.v1.p1.

## SUPPLEMENTAL INFORMATION

Supplemental Information includes Supplemental Experimental Procedures, seven figures, and three tables and can be found with this article online at <http://dx.doi.org/10.1016/j.ccr.2017.01.006>.

## AUTHOR CONTRIBUTIONS

Conceptualization, E.E.G., J.T.P., and C.M.R.; Methodology, E.E.G., B.H.L., V.E.S., E.d.S., N.R., and J.T.P.; Formal analysis: E.E.G., A.N., and J.T.P.; Investigation: E.E.G., B.H.L., V.E.S., L.A.M., P.K.A., P.D., I.K., and N.R.; Resources: T.N., J.S., J.E.C., S.R., A.D., and P.P.M.; Writing – Original Draft, E.E.G., J.T.P., and C.M.R.; Supervision and Funding Acquisition, J.T.P. and C.M.R.

## ACKNOWLEDGMENTS

We thank Ralph Garippa and members of the MSKCC RNAi core facility, and past and present members of the Antitumor Assessment Core Facility for assistance with *in vivo* work, and members of the Molecular Cytology and Pathology core facilities for assistance with TMA construction and automated staining. We acknowledge Madeleine Craske of Active Motif, Inc., for assistance with ChIP-qPCR experiments. We thank all members of the Rudin lab for collaborative efforts. This work was supported by a grant from the LUNGevity Foundation and the American Lung Association (to J.T.P.), a grant from Free To Breathe (to J.T.P.), R01 CA197936-01A1 (to C.M.R.), U54 OD020355 (to E.d.S.), the MSKCC Support Grant/Core Grant P30 CA008748, Conquer Cancer Foundation of ASCO (to B.H.L.), Radiological Society of North America (RR1634) (to B.H.L.), and NIH UL1TR00457 administered by the Clinical and Translational Science Center at Weill Cornell Medical Center and MSKCC (to B.H.L.). This work was supported in part by a VA Merit review I01CX001425-01 (to P.P.M.). Additional research funding was provided by the Van Andel Research Institute through the Van Andel Research Institute – Stand Up To Cancer Epigenetics Dream Team (to C.M.R.). Stand Up To Cancer is a program of the Entertainment Industry Foundation, administered by the American Association for Cancer Research. J.E.C. and S.R. are employees and shareholders of Epizyme, Inc.

Received: August 30, 2016

Revised: November 22, 2016

Accepted: January 17, 2017

Published: February 13, 2017

## REFERENCES

- Alexandrov, L.B., Nik-Zainal, S., Wedge, D.C., Aparicio, S.A., Behjati, S., Biankin, A.V., Bignell, G.R., Bolli, N., Borg, A., Borresen-Dale, A.L., et al. (2013). Signatures of mutational processes in human cancer. *Nature* 500, 415–421.
- Barretina, J., Caponigro, G., Stransky, N., Venkatesan, K., Margolin, A.A., Kim, S., Wilson, C.J., Lehar, J., Kryukov, G.V., Sonkin, D., et al. (2012). The Cancer Cell Line Encyclopedia enables predictive modelling of anticancer drug sensitivity. *Nature* 483, 603–607.
- Beck, B., Lapouge, G., Rorive, S., Drogat, B., Desaedelaere, K., Delafaille, S., Dubois, C., Salmon, I., Willekens, K., Marine, J.C., and Blanpain, C. (2015). Different levels of Twist1 regulate skin tumor initiation, stemness, and progression. *Cell Stem Cell* 16, 67–79.
- Belani, C.P., Dahlberg, S.E., Rudin, C.M., Fleisher, M., Chen, H.X., Takebe, N., Velasco, M.R., Jr., Tester, W.J., Sturtz, K., Hann, C.L., et al. (2016). Vismodegib or cixutumumab in combination with standard chemotherapy for patients with extensive-stage small cell lung cancer: a trial of the ECOG-ACRIN Cancer Research Group (E1508). *Cancer* 122, 2371–2378.
- Carney, D.N., Gazdar, A.F., Bepler, G., Guccion, J.G., Marangos, P.J., Moody, T.W., Zweig, M.H., and Minna, J.D. (1985). Establishment and identification of small cell lung cancer cell lines having classic and variant features. *Cancer Res.* 45, 2913–2923.
- Christensen, C.L., Kwiatkowski, N., Abraham, B.J., Carretero, J., Al-Shahrour, F., Zhang, T., Chipumuro, E., Herter-Spriest, G.S., Akbay, E.A., Altabef, A., et al.

- (2014). Targeting transcriptional addictions in small cell lung cancer with a covalent CDK7 inhibitor. *Cancer Cell* 26, 909–922.
- Daniel, V.C., Marchionni, L., Hierman, J.S., Rhodes, J.T., Devereux, W.L., Rudin, C.M., Yung, R., Parmigiani, G., Dorsch, M., Peacock, C.D., and Watkins, D.N. (2009). A primary xenograft model of small-cell lung cancer reveals irreversible changes in gene expression imposed by culture *in vitro*. *Cancer Res.* 69, 3364–3373.
- De Smet, C., Lurquin, C., Lethe, B., Martelange, V., and Boon, T. (1999). DNA methylation is the primary silencing mechanism for a set of germ line- and tumor-specific genes with a CpG-rich promoter. *Mol. Cell Biol.* 19, 7327–7335.
- Fillmore, C.M., Xu, C., Desai, P.T., Berry, J.M., Rowbotham, S.P., Lin, Y.J., Zhang, H., Marquez, V.E., Hammerman, P.S., Wong, K.K., and Kim, C.F. (2015). EZH2 inhibition sensitizes BRG1 and EGFR mutant lung tumors to Topoll inhibitors. *Nature* 520, 239–242.
- Fischer, K.R., Durrans, A., Lee, S., Sheng, J., Li, F., Wong, S.T., Choi, H., El Rayes, T., Ryu, S., Troeger, J., et al. (2015). Epithelial-to-mesenchymal transition is not required for lung metastasis but contributes to chemoresistance. *Nature* 527, 472–476.
- George, J., Lim, J.S., Jang, S.J., Cun, Y., Ozretic, L., Kong, G., Leenders, F., Lu, X., Fernandez-Cuesta, L., Bosco, G., et al. (2015). Comprehensive genomic profiles of small cell lung cancer. *Nature* 524, 47–53.
- Gerstein, M.B., Kundaje, A., Hariharan, M., Landt, S.G., Yan, K.K., Cheng, C., Mu, X.J., Khurana, E., Rozowsky, J., Alexander, R., et al. (2012). Architecture of the human regulatory network derived from ENCODE data. *Nature* 489, 91–100.
- Horita, N., Yamamoto, M., Sato, T., Tsukahara, T., Nagakura, H., Tashiro, K., Shibata, Y., Watanabe, H., Nagai, K., Inoue, M., et al. (2015). Topotecan for relapsed small-cell lung cancer: systematic review and meta-analysis of 1347 patients. *Sci. Rep.* 5, 15437.
- Jadhav, U., Nalapareddy, K., Saxena, M., O'Neill, N.K., Pinello, L., Yuan, G.C., Orkin, S.H., and Shivdasani, R.A. (2016). Acquired tissue-specific promoter bivalency is a basis for PRC2 necessity in adult cells. *Cell* 165, 1389–1400.
- Kalemkerian, G.P., Akerley, W., Bogner, P., Borghaei, H., Chow, L.Q., Downey, R.J., Gandhi, L., Ganti, A.K., Govindan, R., Grecula, J.C., et al. (2013). Small cell lung cancer. *J. Natl. Compr. Canc. Netw.* 11, 78–98.
- LaFave, L.M., Beguin, W., Koche, R., Teater, M., Spitzer, B., Chramiec, A., Papalex, E., Keller, M.D., Hricik, T., Konstantinoff, K., et al. (2015). Loss of BAP1 function leads to EZH2-dependent transformation. *Nat. Med.* 21, 1344–1349.
- Lin, C.Y., Loven, J., Rahl, P.B., Paran, R.M., Burge, C.B., Bradner, J.E., Lee, T.I., and Young, R.A. (2012). Transcriptional amplification in tumor cells with elevated c-Myc. *Cell* 151, 56–67.
- Lok, B.H., Gardner, E.E., Schneeberger, V.E., Ni, A., Desmeules, P., Rekhtman, N., de Stanchina, E., Teicher, B.A., Riaz, N., Powell, S.N., et al. (2016). PARP inhibitor activity correlates with SLFN11 expression and demonstrates synergy with Temozolomide in small cell lung cancer. *Clin. Cancer Res.* 23, 523–535.
- Loven, J., Hoke, H.A., Lin, C.Y., Lau, A., Orlando, D.A., Vakoc, C.R., Bradner, J.E., Lee, T.I., and Young, R.A. (2013). Selective inhibition of tumor oncogenes by disruption of super-enhancers. *Cell* 153, 320–334.
- Maia, A.M., da Silva, J.H., Mencalha, A.L., Caffarena, E.R., and Abdelhay, E. (2012). Computational modeling of the bHLH domain of the transcription factor TWIST1 and R118C, S144R and K145E mutants. *BMC Bioinformatics* 13, 184.
- McCabe, M.T., Ott, H.M., Ganji, G., Korenchuk, S., Thompson, C., Van Aller, G.S., Liu, Y., Graves, A.P., Della Pietra, A., 3rd, Diaz, E., et al. (2012). EZH2 inhibition as a therapeutic strategy for lymphoma with EZH2-activating mutations. *Nature* 492, 108–112.
- Morschhauser, F., Salles, G., McKay, P., Le Gouill, S., Tilly, H., Radford, J.A., Cartron, G., Dickinson, M.J., Fruchart, C., Gribben, J.G., et al. Initial report from a phase 2 multi-center study of tazemetostat (EPZ-6438), an inhibitor of enhancer of Zeste-Homolog 2 (EZH2), in patients with relapsed or refractory B-cell non-Hodgkin lymphoma (NHL). Presented at the 2016 ASH Meeting on Lymphoma Biology, June 20, 2016; Colorado Springs, CO.
- Mu, Y., Lou, J., Srivastava, M., Zhao, B., Feng, X.H., Liu, T., Chen, J., and Huang, J. (2016). SLFN11 inhibits checkpoint maintenance and homologous recombination repair. *EMBO Rep.* 17, 94–109.
- Nogales, V., Reinhold, W.C., Varma, S., Martinez-Cardus, A., Moutinho, C., Moran, S., Heyn, H., Sebio, A., Barnadas, A., Pommier, Y., and Esteller, M. (2016). Epigenetic inactivation of the putative DNA/RNA helicase SLFN11 in human cancer confers resistance to platinum drugs. *Oncotarget* 7, 3084–3097.
- Park, K.S., Martelotto, L.G., Peifer, M., Sos, M.L., Karnezis, A.N., Mahjoub, M.R., Bernard, K., Conklin, J.F., Szczepny, A., Yuan, J., et al. (2011). A crucial requirement for Hedgehog signaling in small cell lung cancer. *Nat. Med.* 17, 1504–1508.
- Poirier, J.T., Gardner, E.E., Connis, N., Moreira, A.L., de Stanchina, E., Hann, C.L., and Rudin, C.M. (2015). DNA methylation in small cell lung cancer defines distinct disease subtypes and correlates with high expression of EZH2. *Oncogene* 34, 5869–5878.
- Polley, E., Kunkel, M., Evans, D., Silvers, T., Delosh, R., Lauderman, J., Ogle, C., Reinhart, R., Selby, M., Connelly, J., et al. (2016). Small cell lung cancer screen of oncology drugs, investigational agents, and gene and microRNA expression. *J. Natl. Cancer Inst.* 108, <http://dx.doi.org/10.1093/jnci/djw122>.
- Pott, S., and Lieb, J.D. (2015). What are super-enhancers? *Nat. Genet.* 47, 8–12.
- Ribrag, V., Soria, J.-C., Michot, J.-M., Schmitt, A., Postel-Vinay, S., Bijou, F., Coindre, J.-M., Toulemonde, M., Blakemore, S.J., Suttle, B., et al. A phase 1 study of tazemetostat (EPZ-6438), an inhibitor of EZH2: preliminary safety and activity in patients with relapsed or refractory NHL and advanced solid tumors. Presented at the 2016 ASH Meeting on Lymphoma Biology, June 21, 2016; Colorado Springs, CO.
- Rosenthal, R., McGranahan, N., Herrero, J., Taylor, B.S., and Swanton, C. (2016). DeconstructSigs: delineating mutational processes in single tumors distinguishes DNA repair deficiencies and patterns of carcinoma evolution. *Genome Biol.* 17, 31.
- Rudin, C.M., Durinck, S., Stawiski, E.W., Poirier, J.T., Modrusan, Z., Shames, D.S., Bergbower, E.A., Guan, Y., Shin, J., Guillory, J., et al. (2012). Comprehensive genomic analysis identifies SOX2 as a frequently amplified gene in small-cell lung cancer. *Nat. Genet.* 44, 1111–1116.
- Sato, T., Kaneda, A., Tsuji, S., Isagawa, T., Yamamoto, S., Fujita, T., Yamanaka, R., Tanaka, Y., Nukiwa, T., Marquez, V.E., et al. (2013). PRC2 over-expression and PRC2-target gene repression relating to poorer prognosis in small cell lung cancer. *Sci. Rep.* 3, 1911.
- Schmidt, J.M., Panzilius, E., Bartsch, H.S., Irmler, M., Beckers, J., Kari, V., Linnemann, J.R., Dragoi, D., Hirschi, B., Kloos, U.J., et al. (2015). Stem-cell-like properties and epithelial plasticity arise as stable traits after transient Twist1 activation. *Cell Rep.* 10, 131–139.
- Schneeberger, V.E., Allaj, V., Gardner, E.E., Poirier, J.T., and Rudin, C.M. (2016). Quantitation of murine stroma and selective purification of the human tumor component of patient-derived xenografts for genomic analysis. *PLoS One* 11, e0160587.
- Shepherd, F.A., Crowley, J., Van Houtte, P., Postmus, P.E., Carney, D., Chansky, K., Shaikh, Z., Goldstraw, P., and International Association for the Study of Lung Cancer International Staging Committee and Participating Institutions. (2007). The International Association for the Study of Lung Cancer lung cancer staging project: proposals regarding the clinical staging of small cell lung cancer in the forthcoming (seventh) edition of the tumor, node, metastasis classification for lung cancer. *J. Thorac. Oncol.* 2, 1067–1077.
- Sousa, F.G., Matuo, R., Tang, S.W., Rajapakse, V.N., Luna, A., Sander, C., Varma, S., Simon, P.H., Doroshow, J.H., Reinhold, W.C., and Pommier, Y. (2015). Alterations of DNA repair genes in the NCI-60 cell lines and their predictive value for anticancer drug activity. *DNA Repair (Amst)* 28, 107–115.
- Stewart, E., Goshorn, R., Bradley, C., Griffiths, L.M., Benavente, C., Twarog, N.R., Miller, G.M., Caufield, W., Freeman, B.B., 3rd, Bahrami, A., et al.

- (2014). Targeting the DNA repair pathway in Ewing sarcoma. *Cell Rep.* 9, 829–841.
- Tang, S.W., Bilke, S., Cao, L., Murai, J., Sousa, F.G., Yamade, M., Rajapakse, V., Varma, S., Helman, L.J., Khan, J., et al. (2015). SLFN11 is a transcriptional target of EWS-FLI1 and a determinant of drug response in Ewing sarcoma. *Clin. Cancer Res.* 21, 4184–4193.
- Torre, L.A., Bray, F., Siegel, R.L., Ferlay, J., Lortet-Tieulent, J., and Jemal, A. (2015). Global cancer statistics, 2012. *CA Cancer J. Clin.* 65, 87–108.
- Wang, J., Zhuang, J., Iyer, S., Lin, X.Y., Greven, M.C., Kim, B.H., Moore, J., Pierce, B.G., Dong, X., Virgil, D., et al. (2013). Factorbook.org: a Wiki-based database for transcription factor-binding data generated by the ENCODE consortium. *Nucleic Acids Res.* 41, D171–D176.
- Yang, J., Mani, S.A., Donaher, J.L., Ramaswamy, S., Itzykson, R.A., Come, C., Savagner, P., Gitelman, I., Richardson, A., and Weinberg, R.A. (2004). Twist, a master regulator of morphogenesis, plays an essential role in tumor metastasis. *Cell* 117, 927–939.
- Yang, W.H., Lan, H.Y., Huang, C.H., Tai, S.K., Tzeng, C.H., Kao, S.Y., Wu, K.J., Hung, M.C., and Yang, M.H. (2012). RAC1 activation mediates Twist1-induced cancer cell migration. *Nat. Cell Biol.* 14, 366–374.
- Youden, W.J. (1950). Index for rating diagnostic tests. *Cancer* 3, 32–35.
- Zheng, X., Carstens, J.L., Kim, J., Scheible, M., Kaye, J., Sugimoto, H., Wu, C.C., LeBleu, V.S., and Kalluri, R. (2015). Epithelial-to-mesenchymal transition is dispensable for metastasis but induces chemoresistance in pancreatic cancer. *Nature* 527, 525–530.
- Zoppoli, G., Regairaz, M., Leo, E., Reinhold, W.C., Varma, S., Ballestrero, A., Doroshow, J.H., and Pommier, Y. (2012). Putative DNA/RNA helicase Schlafen-11 (SLFN11) sensitizes cancer cells to DNA-damaging agents. *Proc. Natl. Acad. Sci. USA* 109, 15030–15035.

## Supplemental Information

### **Chemosensitive Relapse in Small Cell Lung Cancer**

### **Proceeds through an EZH2-SLFN11 Axis**

**Eric E. Gardner, Benjamin H. Lok, Valentina E. Schneeberger, Patrice Desmeules, Linde A. Miles, Paige K. Arnold, Andy Ni, Inna Khodos, Elisa de Stanchina, Thuyen Nguyen, Julien Sage, John E. Campbell, Scott Ribich, Natasha Rekhtman, Afshin Dowlati, Pierre P. Massion, Charles M. Rudin, and John T. Poirier**

## Supplemental Data

**Table S1 (related to Figure 1). PDX line characteristics used throughout study.**

<b>Text ID</b>	<b>Source</b>	<b>Patient Diagnosis</b>	<b>PDX Diagnosis</b>	<b>Treatment</b>	<b>Site</b>	<b>Reference</b>
JHU-LX22	Johns Hopkins University	SCLC	SCLC	none	pleura	(Hann et al., 2008)
JHU-LX33	Johns Hopkins University	SCLC	SCLC	none	transbronchial	(Hann et al., 2008)
JHU-LX44	Johns Hopkins University	SCLC	SCLC	unknown	unknown	(Poirier et al., 2013)
JHU-LX48	Johns Hopkins University	SCLC	SCLC	platinum	unknown	(Poirier et al., 2013)
JHU-LX101	Johns Hopkins University	SCLC	SCLC	none	transbronchial	(Leong et al., 2014)
JHU-LX102	Johns Hopkins University	SCLC	SCLC	none	transbronchial	(Leong et al., 2014)
JHU-LX108	Johns Hopkins University	SCLC	SCLC	carboplatin, radiation	transbronchial	(Leong et al., 2014)
JHU-LX110	Johns Hopkins University	SCLC	SCLC	none	transbronchial	(Leong et al., 2014)
SCRX-Lu149	StemcentRx, Inc.	SCLC	SCLC	none	lung	(Saunders et al., 2015)
MSK-LX40	Memorial Sloan Kettering Cancer Center	SCLC	SCLC	C/E	lung	new
MSK-LX95	Memorial Sloan Kettering Cancer Center	SCLC	SCLC	C/E	lung	new

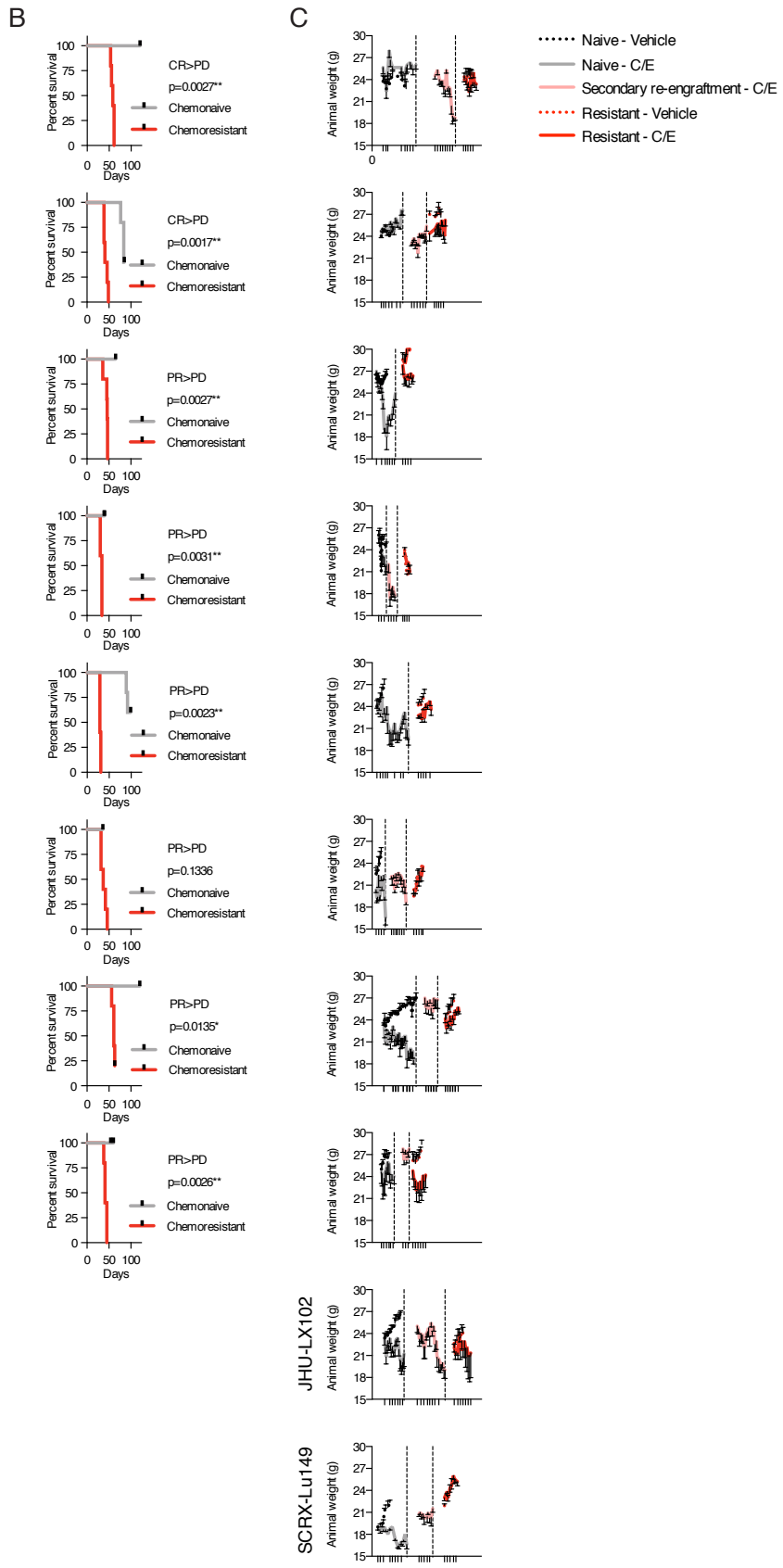
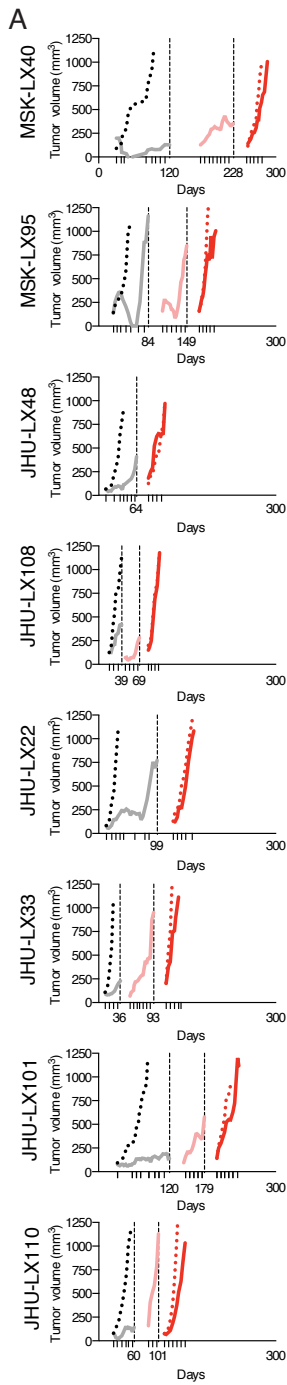


**Figure S1 (related to Figure 1). Modeling acquired resistance to C/E in PDX models of SCLC.**

(A) Average tumor volume curves for 10 models included in study. n=5/arm, per PDX. Data per treatment group reported as means for clarity. Dashed lines indicate points on study where cisplatin/etoposide (C/E) treated cohorts were collected and re-engrafted (pooled fashion) into additional cohorts of animals. JHU-LX102 and SCR-Lu149 data were included in Figure 1C, thus are omitted in these panels. Color legend for entire figure on far right.

(B) Survival for chemonaive and chemoresistant versions of models on C/E treatment. Model chemosensitivity conversion status (>) indicated above p values from log-rank (Mantle-Cox) tests; CR=complete response, PR=partial response, PD=progressive disease. Survival is shown as time on study to reach the pre-specified volumetric endpoint of 1,000 mm<sup>3</sup>. Survival data points were censored if volumetric endpoints were not reached on protocol (~1,000 mm<sup>3</sup>), serious weight loss was encountered (>20% body weight at point of randomization), or total cycles of C/E reached tolerability endpoint (~8 weekly cycles).

(C) Animal weights on study. Data are reported as mean ± SEM; n=5/arm.

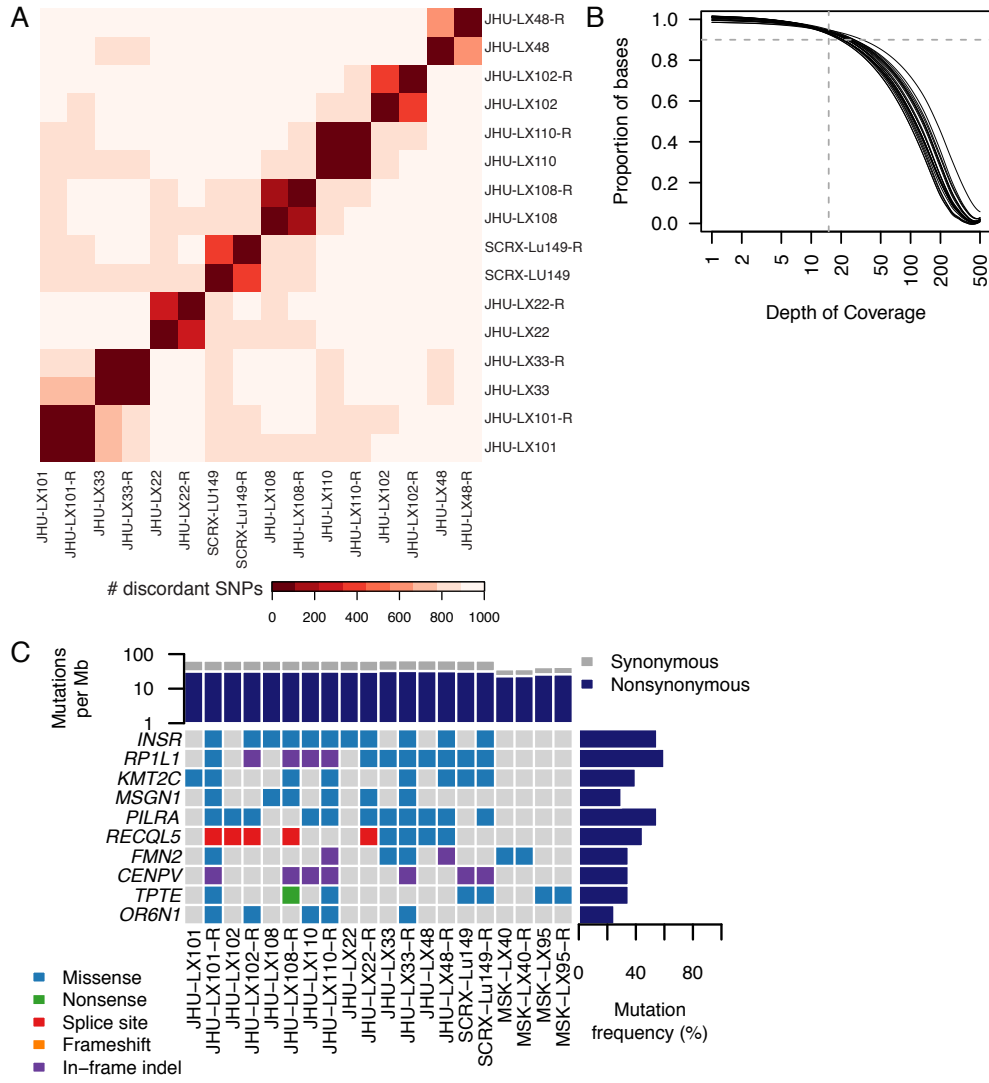


**Figure S2 (related to Figure 2). Whole exome sequencing of paired naive and resistant PDX pairs.**

(A) Concordance of genotypes for >1,000 common single nucleotide polymorphisms (SNPs) across naive and resistant pairs. Color scale below.

(B) Proportion of bases in the exome capture region covered to a given read depth. The intersection of the horizontal (90%) and the vertical lines (15) indicate the minimum depth used to call mutations using MuTect2.

(C) A mutation plot indicating the most common mutations occurring in the chemoresistant setting ordered by frequency. Mutation legend shown below.

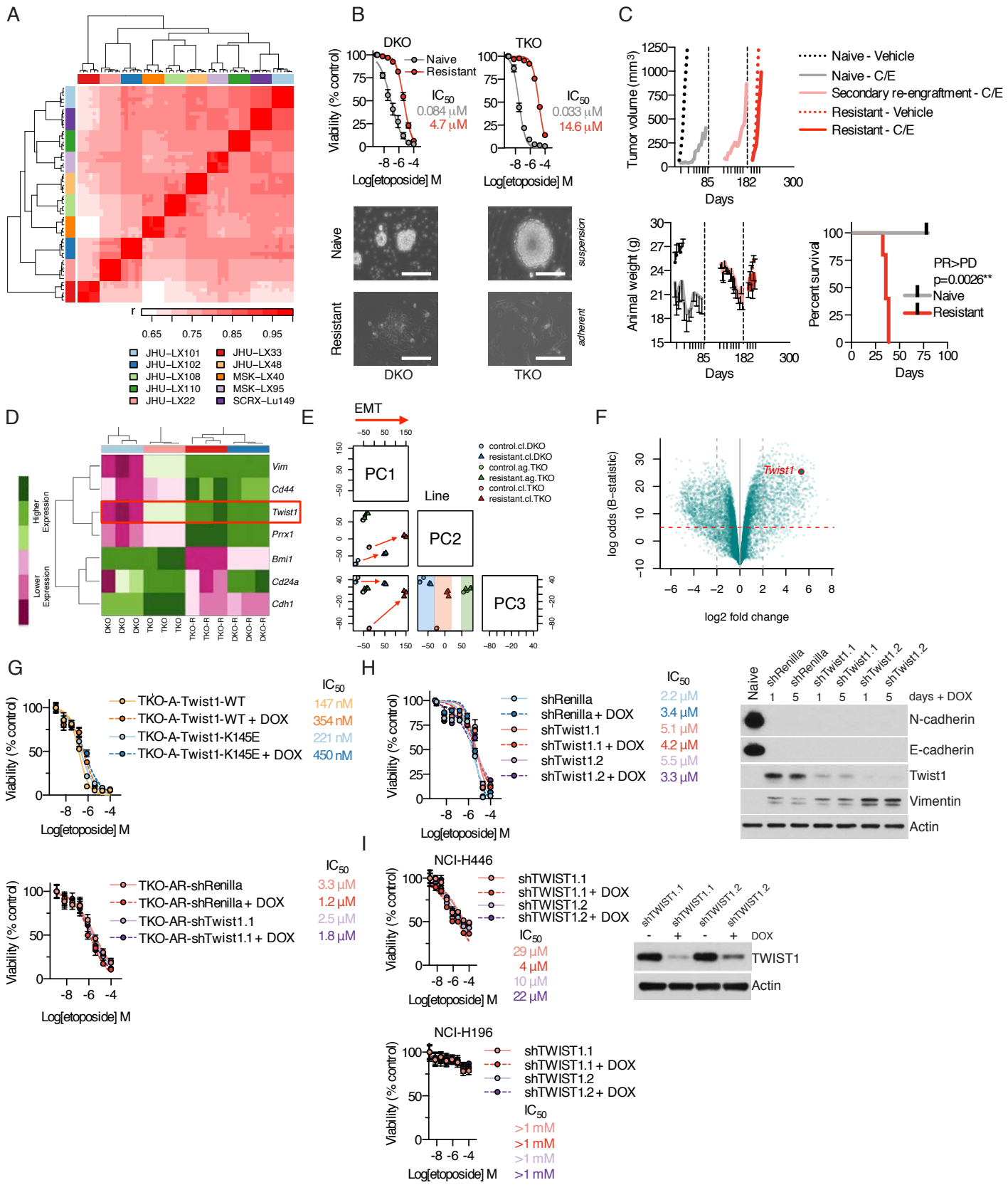


**Figure S3 (related to Figure 3). TWIST1 is upregulated in multiple models of chemoresistant SCLC.**

- (A) Hierarchical clustering of correlation coefficients,  $r$ , from RNA-seq data on biological triplicates of chemonaive and chemoresistant paired PDX samples.  $n=3$  replicates per model per setting;  $n=60$  data columns/rows. Color legend and scale below.
- (B) Shift in etoposide sensitivity from in vitro acquired resistance modeling in DKO and TKO mSCLC cell lines. Change in morphologic appearance and culture conditions of chemonaive (suspension/spheroid) and chemoresistant (adherent) cell lines. Scale bars set to 200  $\mu$ m. Experimental results are shown for 72 hr post-dose of etoposide;  $n=3$ /data point; mean viability  $\pm$  SEM.
- (C) Average tumor volume plot for triple knock-out allograft (TKO-A) mSCLC model; treatment arms indicated in legend on right. Points of re-transplant are indicated along the x-axis with vertical dashed lines. Day 1 of C/E cycles are indicated as vertical ticks along the x-axis. The same schedule and treatment criteria of C/E used to generate chemoresistant PDXs was used to generate chemoresistant TKO-A (TKO-AR). Below: Average animal weights on study  $\pm$  SEM;  $n=5$ /arm. Below right: survival of naive versus resistant C/E-treated cohorts of mSCLC TKO allograft (TKO-A) models. Model conversion from partial response (PR) to progressive disease (PD) indicated in margin.  $P$  value from log-rank (Mantle-Cox) test.
- (D) Relative expression for select genes involved in EMT between naive or parental (P) and resistant (R) cell lines, calling out *Twist1* (red box). Gene expression intensity legend on far left.
- (E) Principal component (PC) analysis for naive and resistant versions of mSCLC models broken down by component. The first component of epithelial-mesenchymal transition (EMT) is shown. Legend colors and shapes shown for cell lines (cl) and allograft (ag).
- (F) Volcano plot for differential gene expression across all mSCLC paired naive/parental as compared to resistant models (pooled analysis). Significance of differential expression (dashed vertical line; log<sub>2</sub> fold change  $>2$ ) and log odds beta (B) statistic (red dashed horizontal line; 5) indicated on plot. *Twist1* data point highlighted in red.
- (G) Conditional gain of *Twist1* or the K145E DNA-binding mutant of *Twist1* in the naive setting or conditional suppression of *Twist1* in the resistant setting of the TKO allograft (TKO-A/AR) and influence on chemosensitivity. Conditional expression was initiated when doxycycline (DOX) was added to the culture media at 1  $\mu$ g/mL, every other day, for 5 days before re-plating for viability experiments. Experimental results are shown for 72 hr post-dose of etoposide.  $n=3$ /data point, mean  $\pm$  SEM.
- (H) Conditional suppression of *Twist1* in the resistant DKO cell line (DKO-R) and influence on chemosensitivity. Experimental results shown for 72 hr post-dose of etoposide.  $n=3$ /data point, mean  $\pm$  SEM. On right, conditional suppression of *Twist1* and effects on EMT-associated changes in protein expression of E-cadherin, N-cadherin and vimentin. Western blots for resistant DKO (DKO-R) cells on doxycycline (1  $\mu$ g/mL) for 1 or 5 days before collection of samples for Western blot.
- (I) Conditional suppression of *TWIST1*<sup>HIGH</sup> in the *TWIST1*<sup>HIGH</sup> human SCLC cell lines NCI-H446 and NCI-H196 and influence on sensitivity to etoposide. Doxycycline (DOX) was added to the culture media at 1  $\mu$ g/mL every other day for 5 days before re-plating for viability experiments. Experimental results are shown for 72 hr post-dose of etoposide. Two independent *TWIST1* shRNAs were tested for target suppression at 72 hr after a single dose (1  $\mu$ g/mL) of doxycycline (DOX) in NCI-H446, using shTWIST1.1 for both conditional cell line experiments.  $n=3$ /data point, mean  $\pm$  SEM.

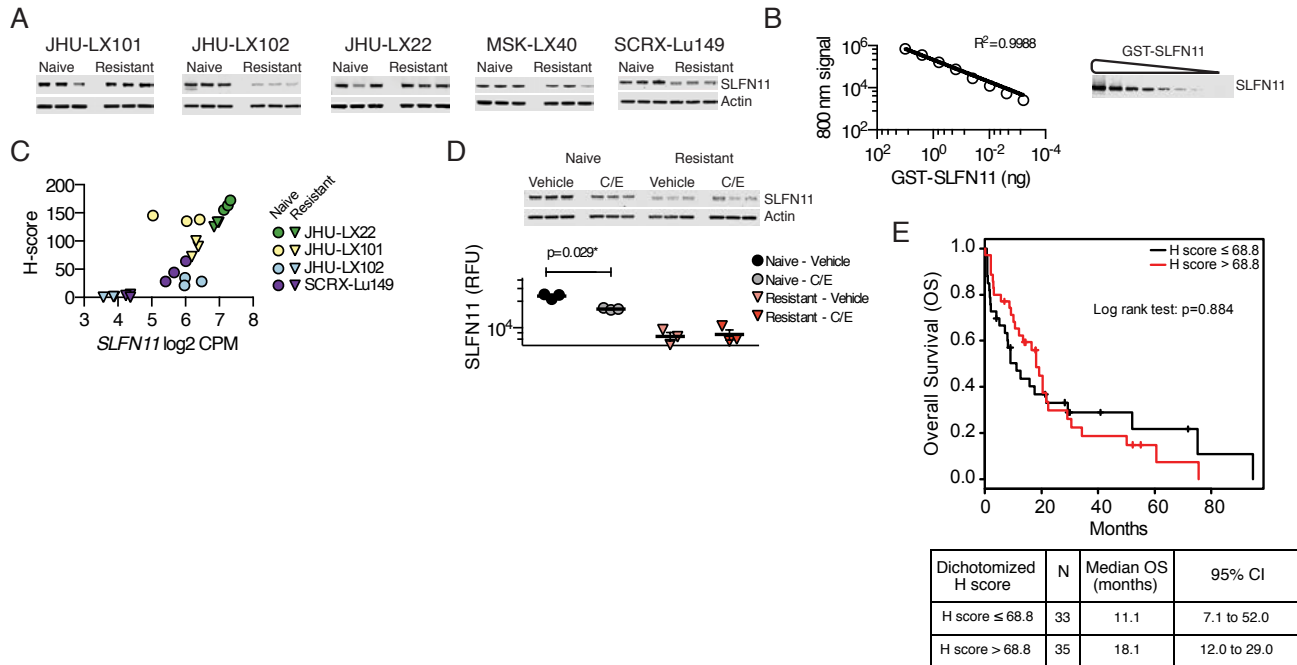


**Figure S4 (related to Figure 4). SLFN11 is downregulated in multiple models of chemoresistant SCLC.**

(A) Western blot images from triplicate chemonaive and resistant PDX tumor samples used for calculating data included in Figure 4G, normalizing SLFN11 signal (800 nm) to actin (700 nm). Three tumor replicates analyzed per setting.

(B) Standard curve for detection of recombinant SLFN11 establishes conservative upper and lower limits of detection in pure versus crude experimental samples; recombinant GST-tagged SLFN11 (GST-SLFN11). Standard curve  $R^2$  value of 0.9988.

(C) RNA-seq versus SLFN11 H-score for available PDX naive and resistant tumors. Paired triplicates are color-coded in the naive (circles) or resistant (downward triangle) and correspond to the color grid use in Figure 3A.

(D) Change in tumor SLFN11 expression from vehicle or C/E-treated arms of chemonaive or chemoresistant SCRX-Lu149 model. SLFN11 relative fluorescence units (RFU) as a function on time on treatment in PDX model SCRX-Lu149. P value shown for paired t-test. Mean  $\pm$  SD.

(E) Survival of SCLC by dichotomized H-score. The best cutoff of H-score for predicting objective response rate (ORR) is 68.8 based on maximizing the Youden's J index ( $J = \text{sensitivity} + \text{specificity} - 1$ ). Inset table below shows usable clinical cases from H-score on TMAs analyzed in aggregate.

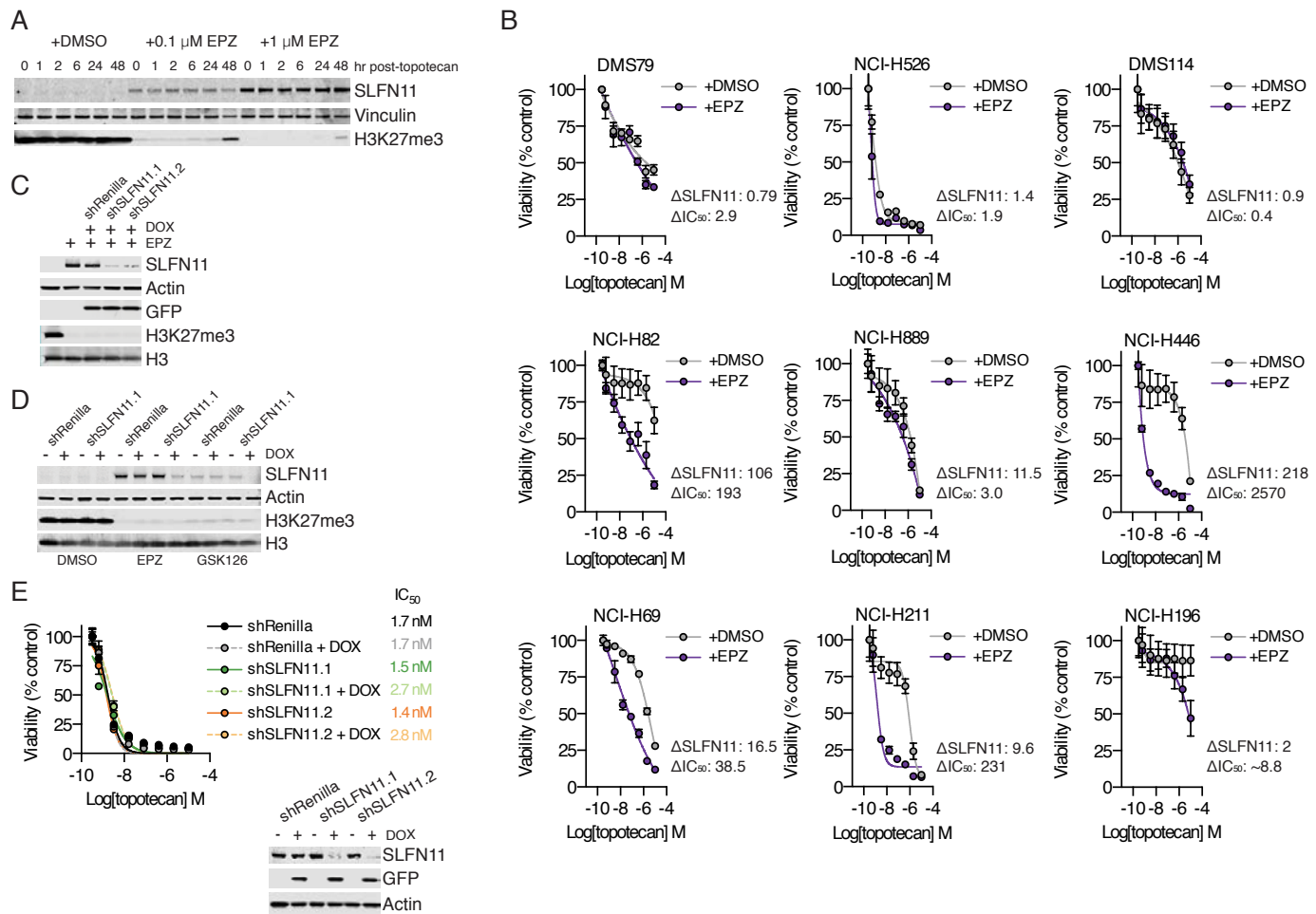


**Figure S5 (related to Figure 5). SLFN11 is re-expressed in SCLC following chemical EZH2 inhibition.**

(A) NCI-H82 cell line was treated for 7 days with DMSO, 100 nM or 1  $\mu$ M EPZ in culture, adding EPZ every day. Cells were then exposed to 1  $\mu$ M topotecan for 1 hr, washed and then released into fresh media for a 48 hr collection period. Indicated time points in hours shown above for Western blot.

(B) Individual IC<sub>50</sub> curve traces for the 9 human SCLC cell lines used for plotting data in Figure 5G. Cells were split every 3 days, adding 1  $\mu$ M EPZ or vehicle (DMSO) every day for 7 days, before plating 1-5x10<sup>4</sup> cells for determining 72 hr viability. Changes in SLFN11 protein expression and best fits of topotecan IC<sub>50</sub> values shown per cell line. n=3/data point, mean  $\pm$  SEM. Experiments were repeated three times, with a representative set of replicates shown.

(C) NCI-H82 treated with 1  $\mu$ M EPZ in culture for 7 days with or without a 72 hr co-treatment period with 1  $\mu$ g/mL doxycycline (DOX). Two independent shRNAs targeting SLFN11 are shown (shSLFN11.1 and shSLFN11.2) versus a non-targeting shRenilla control.

(D) SLFN11 re-expression under different EZH2 chemical inhibitors. NCI-H82 treated in culture for 7 days with DMSO, 1  $\mu$ M EPZ or 1  $\mu$ M GSK126 with or without a 72 hr co-treatment period with 1  $\mu$ g/mL doxycycline (DOX) to induce shRNA against SLFN11 or Renilla luciferase before analyzing by Western blot.

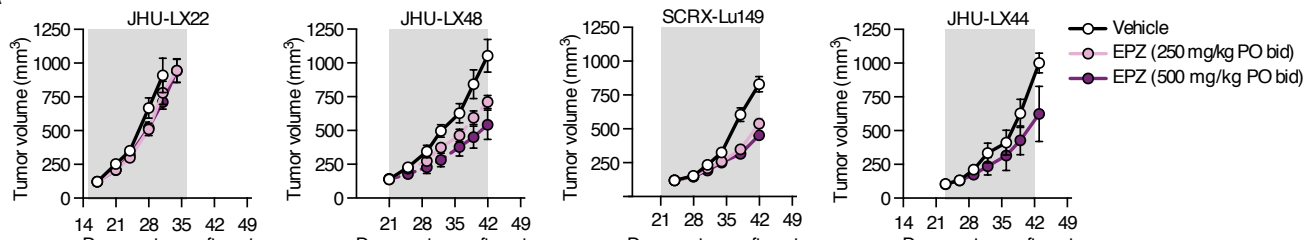
(E) Conditional shRNA suppression of SLFN11 in the SLFN11<sup>HIGH</sup> SCLC cell line NCI-H526 and effect on chemosensitivity. As in Figure 5H, 1  $\mu$ g/mL doxycycline (DOX) was added to cell lines for 3 days before re-plating for viability assays. IC<sub>50</sub> values colored according to arm. Two independent shRNAs against SLFN11 were tested prior to experiments (shSLFN11.1 and shSLFN11.2) as well as an shRNA targeting Renilla luciferase (shRenilla) shown in Western blot. GFP is co-expressed from an independent promoter upon exposure to doxycycline in pLT3GEPIR, which was the common backbone for all shRNA experiments (Fellmann et al., 2013). n=3/data point, mean  $\pm$  SEM.

**Table S2 (related to Figure 6). Summary of described resistance mechanisms observed in PDX models and efficacy of chemical EZH2 inhibition.**

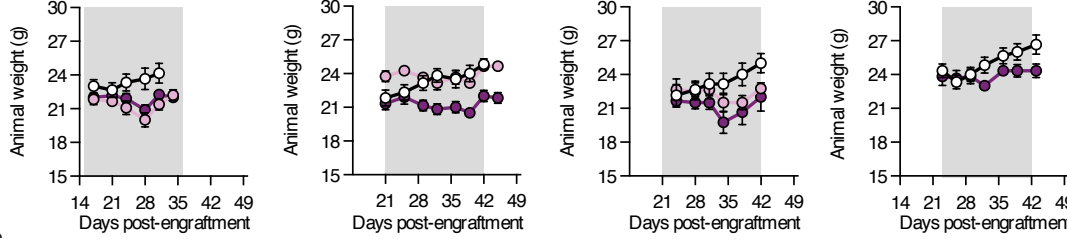
PDX	Chemonaive C/E response	Chemoresistant C/E Response	<i>TWIST1</i>	<i>SLFN11</i>	EPZ efficacy
JHU-LX22	PR	PD	-	decrease	NR
JHU-LX33	PR	NR	increase	-	-
JHU-LX44	NR	NR	-	-	PR
JHU-LX48	PR	PD	-	-	PR
JHU-LX101	PR	PD	-	-	-
JHU-LX102	PD	PD	-	decrease	PR
JHU-LX108	PR	PD	increase	-	NR
JHU-LX110	PR	PR	-	-	-
MSK-LX40	CR	PD	-	decrease	-
MSK-LX95	CR	PD	increase	-	-
SCRX-Lu149	PR	PD	-	decrease	PR

CR=complete response, PR=partial response, PD=progressive disease, NR=no response

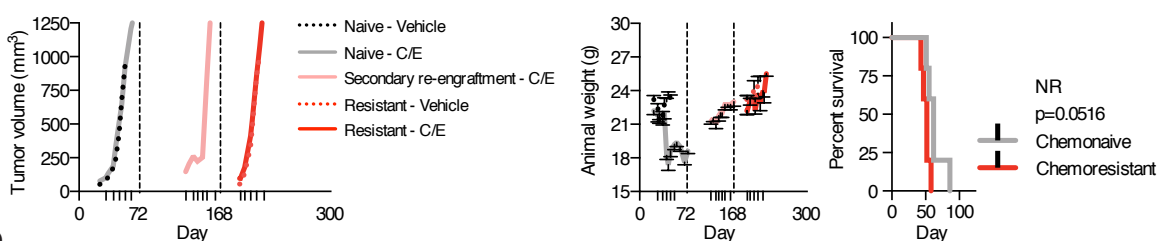
A



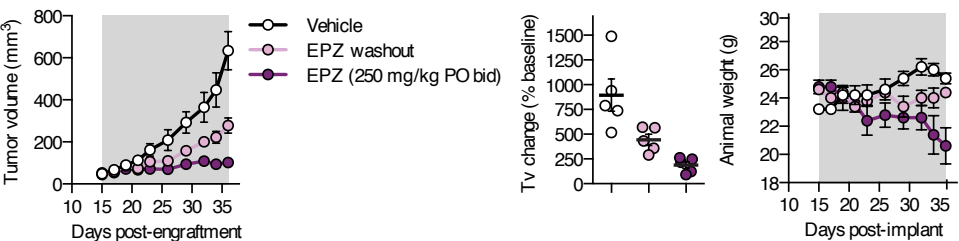
B



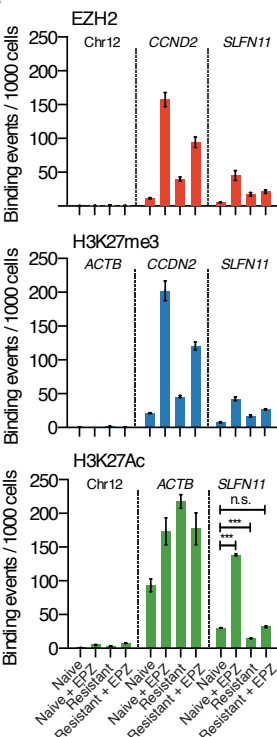
C



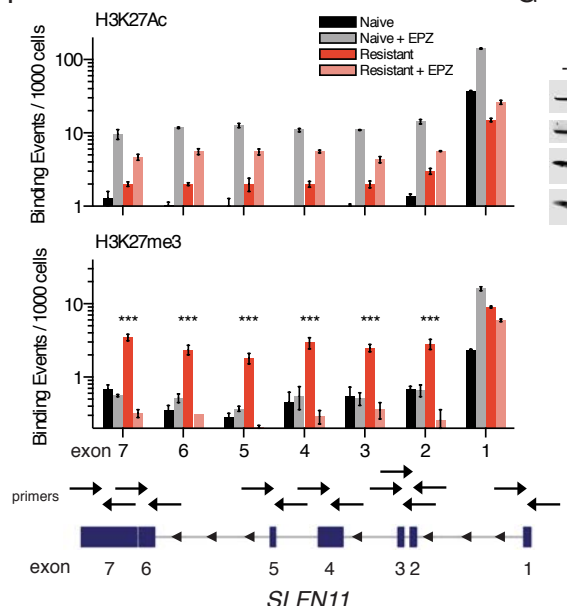
D



E



F



G

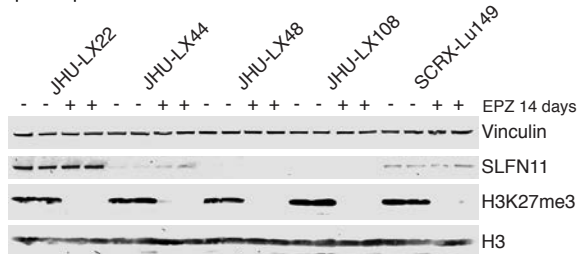


**Figure S6 (related to Figure 6). EZH2 chemical inhibition restores *SLFN11* expression after silencing during acquired resistance.**

(A) Single agent activity of EPZ across four PDX models, using two separate dose schedules. Areas in grey represent time on continuous oral, twice a day (PO bid) treatment. EPZ was administered on a 10 AM/6 PM schedule, 7 days a week for 14-21 days, depending on tumor growth kinetics during treatment. Tumor volumes reported as mean  $\pm$  SEM; n=7-8 per arm. The 250 mg/kg PO bid arm for JHU-LX44 was not performed. All tumors used for these experiments were of chemonaive origin, where applicable.

(B) Average weight  $\pm$  SEM for animals in (A).

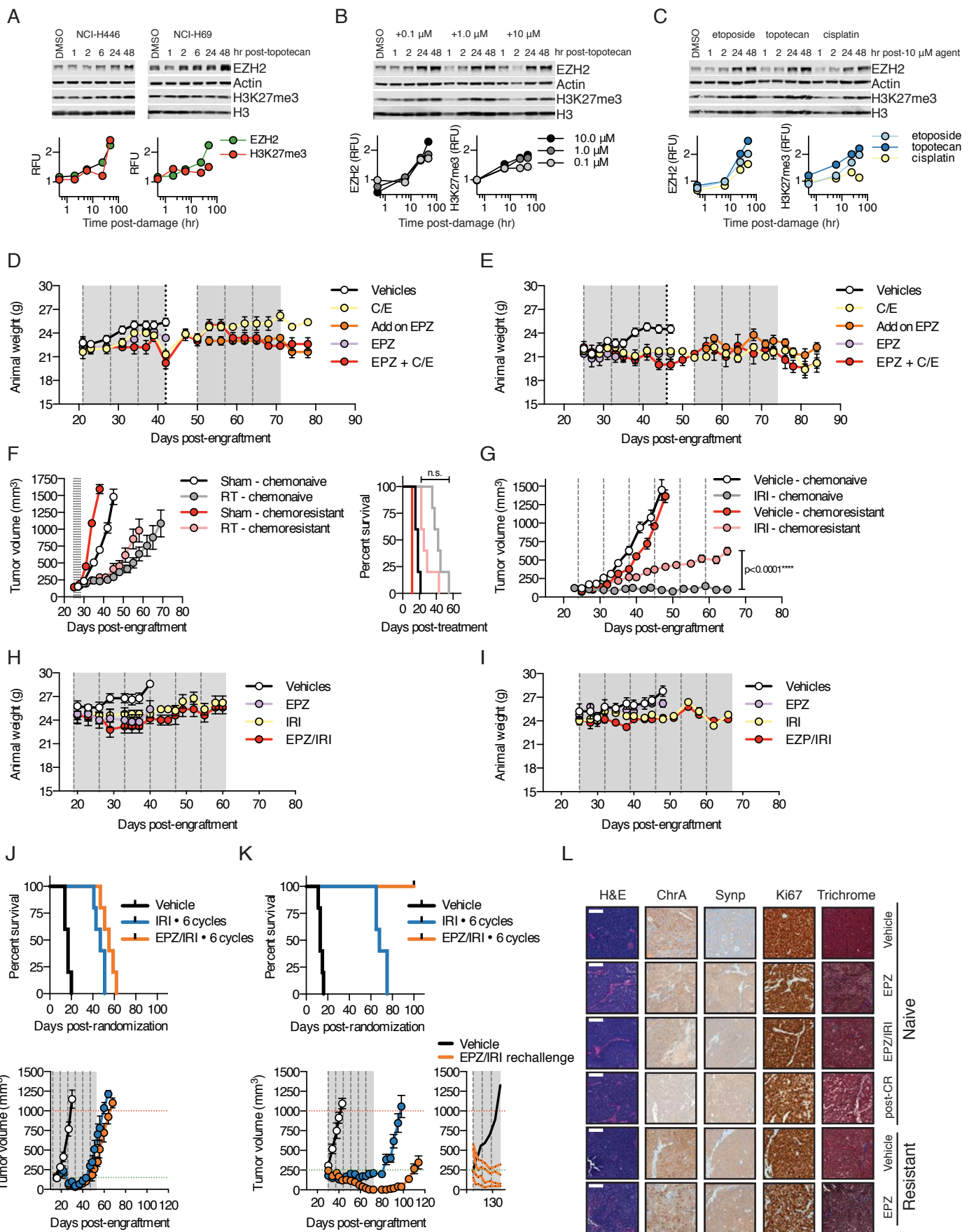
(C) C/E efficacy in chemorefractory model JHU-LX44. Mean tumor volume  $\pm$  SEM (n=5/arm), animal weights, and survival as a function of time to reach a volumetric endpoint of 1,000 mm<sup>3</sup> as in Figure 1 and S1. Color legend on right.

(D) Repeated exposure to EPZ in vivo in SCRX-Lu149. Left: efficacy of continuous dosing through a re-engraftment period. Tumors at the end of a three-week efficacy experiment for SCRX-Lu149 (from Figure S6A) were engrafted from either vehicle or 250 mg/kg PO bid treatment arms into mice. Two weeks following engraftment, mice from previously treated tumors were treated with vehicle (washout) or EPZ for an 3 additional weeks; Data reported as average tumor volume  $\pm$  SEM; n=5/arm. Color legend used for panel on right. Middle: Comparison of tumor volume change (Tv change) at week 3 on treatment versus volumes at treatment initiation (baseline) per group. Individual Tv change points shown with mean  $\pm$  SEM per indicated arm. Right: Average animal weight on study for left panel. Continuous treatment arm approached limits of protocol weight loss (~20% body weight from randomization).

(E) ChIP-qPCR for *SLFN11* (upstream of first exon) in various tumor samples use in Figure 6 as compared to positive and negative control primer pairs. ChIP target indicated in color: EZH2 (red), H3K27me3 (blue) and H3K27Ac (green). Each ChIP-qPCR series is shown for three targets in the order of negative control, positive control and *SLFN11* (left-to-right): Chr12 refers to a gene desert region in chromosome 12, not known to bind any transcription factor (Active Motif; 71001). P value indices (\*\*<0.0001) reported for paired t-tests between groups within the H3K27Ac (green) sample set; n.s.=non-significant; n=3 replicates per condition, mean  $\pm$  SD.

(F) ChIP-qPCR for *SLFN11* in an exon-by-exon fashion in various tumor samples use in Figure 6. ChIP targets H3K27Ac (above) and H3K27me3 (below). Indicated exons along bottom x-axis. n=3 replicates per condition, mean  $\pm$  SD. P value indices (\*\*<0.0001) reported for paired t-tests between resistant SCRX-Lu149 samples and all other sample test sets; n.s.=non-significant. Exon model for *SLFN11* locus shown below with indicated primer pairs used to interrogate specific exons. Exon model used for illustrative purposes and not to any scale.

(G) Western blot analysis from 5 chemonaive PDX models treated with vehicle (-) or 250 mg/kg EPZ PO bid (+) for 14 days before collection of tissues. Two tumors examined per arm, per PDX at day 14 on study.



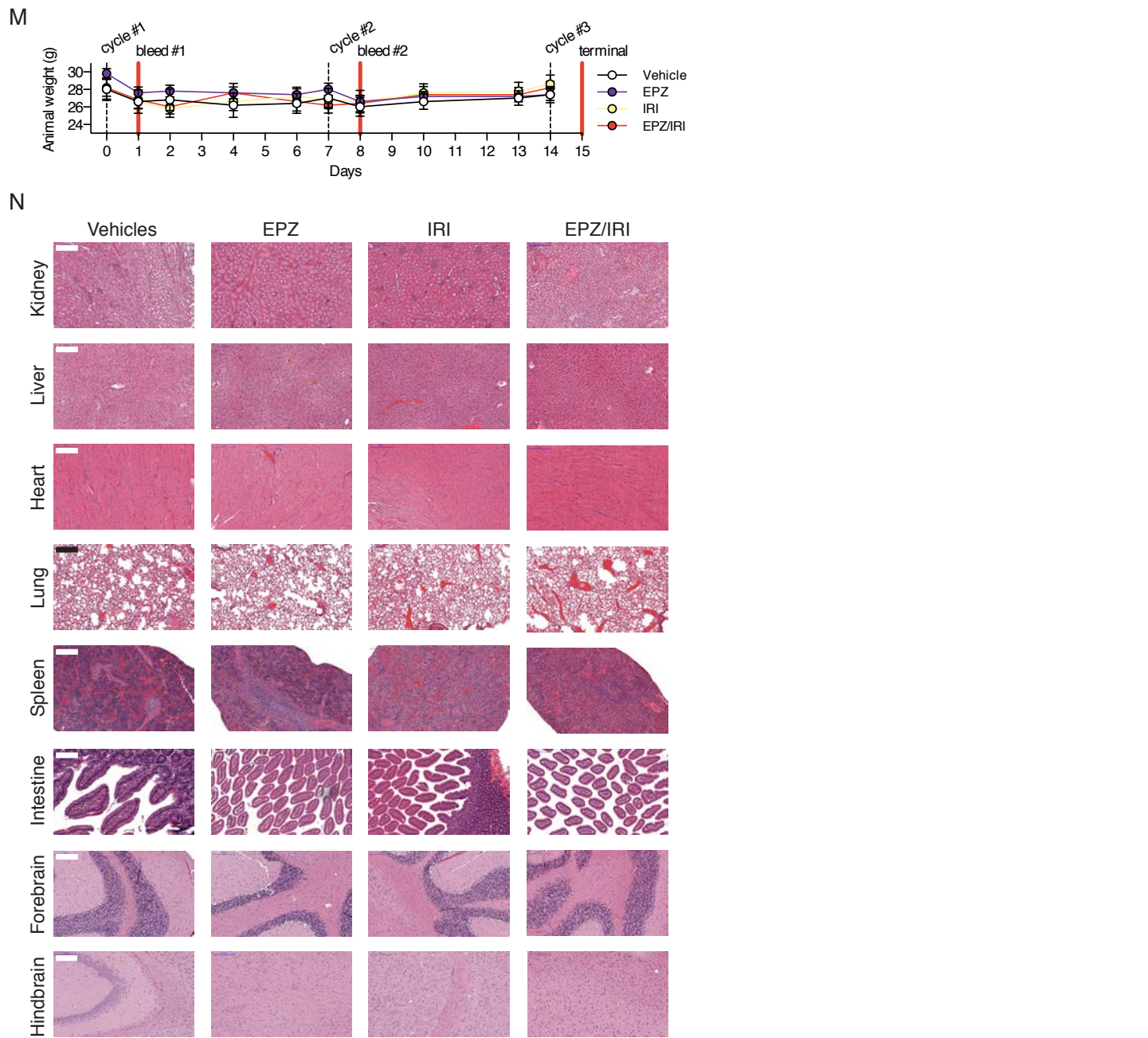


**Figure S7 (related to Figure 7). Combining EPZ with chemotherapy is an effective and safe therapeutic strategy in SCLC.**

(A) Quantitation of EZH2 and H3K27me3 in SCLC cell lines NCI-H446 and NCI-H69 following DNA damage. EZH2 signal normalized to actin and H3K27me3 normalized to total H3. Cells exposed to 1  $\mu$ M topotecan for 1 hr and then washed and released into fresh media. Cells were collected at indicated time points for Western blot. Relative fluorescence units (RFU) per targets interrogated as shown.

(B) Quantitation of EZH2 and H3K27me3 following dose-dependent DNA damage in NCI-H446. Damage induced as in (A) using indicated doses of topotecan and then collected at time points for Western blot. Data normalized to undamaged control at 48 hr. EZH2 and H3K27me3 relative fluorescence units (RFU) shown per time point.

(C) Effect of type of DNA damaging agent on EZH2 and H3K27me3 in NCI-H446. Damage induced as in (A) using indicated doses of compounds. EZH2 and H3K27me3 relative fluorescence units (RFU) shown per time point

(D) Average animal weights on study for Figure 7D  $\pm$  SEM for each treatment arm indicated. n=5/arm.

(E) Average animal weights on study for Figure 7E  $\pm$  SEM for each treatment arm indicated. n=5/arm.

(F) Efficacy of ionizing radiation upon acquired resistance to C/E. Chemonaive and chemoresistant versions of SCRX-Lu149 received 2 Gy (abbreviated RT) or sham irradiation for 4 consecutive days and tumor volumes were recorded during outgrowth; Mean volume  $\pm$  SEM; n=5-6/arm. Survival reported as time post-treatment to reach a volumetric endpoint of 1,000 mm<sup>3</sup>. n.s.=non-significant by log-rank (Mantle-Cox) test.

(G) Efficacy of irinotecan upon acquired resistance to C/E. Chemonaive and chemoresistant versions of SCRX-Lu149 received weekly cycles of irinotecan (100 mg/kg IP every 7 days) or vehicle for 6 consecutive weeks and tumor volumes were recorded. Dashed horizontal lines indicate day 1 of a weekly cycle. Mean volume ± SEM; n=5/arm. P value shown for paired t-test.

(H) Average animal weights on study for Figure 7F ± SEM for each treatment arm indicated; n=5/arm.

(I) Average animal weights on study for Figure 7G ± SEM for each treatment arm indicated; n=5/arm.

(J) Efficacy of combined irinotecan (IRI) and EPZ (EPZ/IRI) in the SLFN11<sup>LOW</sup> chemonaive model JHU-LX108. Survival curve shown above; event/endpoint is time to tumor volume reaching 1,000 mm<sup>3</sup> post-randomization (on treatment). Randomizing starting volume (green dotted line) and endpoint volume (red dotted line) are indicated horizontally on tumor growth curves. Dashed lines represent day 1 of a weekly cycle, with grey area indicating time on treatment; Mean volume ± SEM; n=5/arm.

(K) Efficacy of combined irinotecan (IRI) and EPZ (EPZ/IRI) in the SLFN11<sup>HIGH</sup> chemonaive model JHU-LX102 as in Figure S7J. Inset: 4/5 animals were re-treated with 3 cycles of EPZ/IRI after recurring from complete responses (individual orange lines), treating the median volume recurrence animals with vehicle only (black line) and monitoring outgrowth.

(L) Immunohistochemistry on paired chemonaive and chemoresistant JHU-LX102 samples treated with EPZ alone or in combination with IRI. ChrA=chromogranin A, Synp=synaptophysin, Trichrome=Masson's trichrome. Scale bar on H&E panel set to 100 µm and equivalent throughout panels. All vehicle, EPZ or EPZ/IRI tumors were treated continuously for 21 days. The post-complete response (CR) tumor was the vehicle-treated median outgrowth tumor from Figure S7K inset. Three tumors were analyzed per arm by a pathologist blinded to treatment group, with the exception of the post-CR tumor (n=1). Shown are representative images from one animal per group.

(M) Schematic outline of EPZ ± IRI toxicity studies performed in 10-12 week old female NSG mice. Animal weights reported as means ± SEM; treatment arms color legend on far right. Cycles of irinotecan (dashed vertical lines; 100 mg/kg IP) were given 24 hr before tail vein bleeds, where bleeds are indicated by solid, vertical red lines. Following the final cycle of irinotecan (cycle #3), all animals were taken for gross necropsy and histologic analysis; n=5/arm.

(N) Representative H&E images of major organs examined for treatment-related toxicities. Scale bars (200 µm) are indicated on vehicle arm images and equivalent throughout panels; n=5/arm.

**Table S3 (related to Figure 7). Blood chemistry for toxicity analysis of EPZ ± IRI in non-tumor bearing NSG female mice.**  
Provided as an excel file.

## SUPPLEMENTAL EXPERIMENTAL PROCEDURES

### In vitro and in vivo generation of acquired resistance to cisplatin/etoposide

Mouse DKO and TKO cells were cultured under increasing concentrations of etoposide, refreshing media and drug twice weekly, until stable cultures were capable of proliferating in the presence of 1 µM etoposide. Parental and resistant versions of the DKO and TKO cell lines were confirmed by STR, as lines were in continuous culture for ~6 months. In vivo, cohorts of tumor-bearing animals were challenged weekly with cycles of cisplatin (5 mg/kg IP day 1) and etoposide (8 mg/kg IP days 1-3) as long as the following conditions were met: 1) tumor volumes were greater than 100 mm<sup>3</sup> and 2) animals did not lose >20% body weight when compared to the body weights at the point of randomization (starting weights). On the morning of day 1 of each weekly cycle, animals were given 0.8-1.0 ml of normal saline subcutaneously to facilitate renal clearance of the cisplatin, as cumulative dehydration from cisplatin was the dose-limiting toxicity of this schedule. Where toxicity (usually uniform within a treatment cohort) was encountered, animals were given one week of holiday from treatment to allow recovery of weight. All NSG animals were maintained on Sulfatrim® diet throughout the period of study.

### mSCLC triple knock-out allograft (TKO-A)

All in vivo mSCLC experiments were performed using an allograft of the triple (*Rb1/Trp53/Rbl2*) knockout mouse model of SCLC (Jahchan et al., 2013) maintained in female, 2-3 month old athymic nude mice (Envigo; Hsd:Athymic Nude-Foxn1nu). Flank tumors were engrafted and maintained as described for PDX models, with the exception of using a mouse tumor dissociation kit to process these tumors into single cell suspensions (Miltenyi; 130-096-730).

### Tumor Micro Array (TMA) construction and immunohistochemistry

Tumor cores were obtained from embedded PDX tumors tissue in donor blocks using a 1 mm biopsy punch needle (IHC World; W-125-0) then embedded/inserted into paraffin recipient block/negative mold (IHC World; 10\*17 Quick Ray mold IW-UM01-1). Empty slots were filled with blank paraffin cores. All cores were gently tamped down using biopsy punch needle then the entire block was placed face down on a glass slides and heated to 50 C for 2 hr to merge donor cores with the recipient block. Block and glass slide were then placed on ice for 30 min before sectioning. Two tissue microarrays (TMAs) made of primary and metastatic SCLC specimens were prepared from formalin-fixed paraffin-embedded (FFPE) tissue blocks following previously reported methods (Kononen et al., 1998; Ocak et al., 2010). Pathology blocks were retrieved from the archives of the Department of Pathology at Vanderbilt University Medical Center, Nashville VA Medical Center and St-Thomas Hospital in Nashville, Tennessee. They were obtained between 1996 and 2008 from patients who had surgery or bronchoscopy prior to medical treatment. SCLC diagnosis was confirmed on hematoxylin and eosin-stained (H&E) sections by an experienced lung cancer pathologist. Treatment was administered on an individualized basis according to disease stage and patient performance status (PS) as per standard of care therapy (chemotherapy and radiotherapy). All patients were followed through chart review until death or until data analysis of this manuscript. Clinical data were obtained from tumor registry and hospital charts. Studies to collect tissues were approved with patient consent and by the Institutional Review Boards at each medical center involved. Staining and H-score calculations, a weighed score that ranges from 0 - 300 and integrates IHC staining intensity and area, was performed as previously described (Lok et al., 2016).

### Cell culture, in vitro viability assays and chemical inhibitors

All cell lines were obtained from the American Type Culture Collection (ATCC), were confirmed by STR (DDC Medical) and tested negative for mycoplasma (Lonza MycoAlert PLUS; LT07-710) within 6 months of use. All cell lines were maintained in RPMI-1640 supplemented with 10% FBS, 2 mM L-glutamine and 1x penicillin/streptomycin. Ex vivo cell culture of PDX tumors was performed as previously described (Poirier et al., 2015). EPZ011989 (abbreviated EPZ within text) was provided by Epizyme and formulated as previously described (Campbell et al., 2015). Cisplatin (APP), etoposide (Teva) and irinotecan (Hospira) for in vivo use were obtained from the MSKCC hospital pharmacy and formulated in normal saline immediately before use. Topotecan (Selleck Chem), GSK126 (Selleck Chem) and 5-azacitidine (Sigma) were purchased commercially and formulated in DMSO. Cell viability experiments were performed at 72 hr post-dosing, unless indicated otherwise within the text, where 1-5x10<sup>4</sup> viable cells were seeded in 100 µL/well of fresh media in black 96-well plates and drugs added to a final volume of 200 µL/well one day after seeding plates (Corning; 3916). Cell viability experiments were monitored using AlamarBlue (Life Technologies), allowing the reagent to develop overnight (~16 hr) before reading plates on a compatible plate reader (BioTek; Synergy Neo). Throughout the text DMSO is used as the vehicle control for in vitro or ex vivo experiments.

### Plasmids and generation of lentiviral supernatants

SLFN11 (HsCD00082389) and human TWIST1 (HsCD00042456) cDNAs in pDONR vectors were purchased from DNASU plasmid repository. Mouse Twist1 cDNA was purchased from Origene (MR227370). Polymerase chain reactions (PCRs) were performed using a GeneAmp PCR System 9700 Thermocycler (Applied Biosystems). Competent Stbl3 cells were purchased from Invitrogen. Plasmids were isolated and purified from bacteria using QIAquick Spin Miniprep Kit (Qiagen). SLFN11 was cloned into plasmid pDONR221 (Life Technologies). Using primers with the following sequences 5'-TGATGATAATGATACCCAGCTTCTTGACAAAGTGGCATT-3' and 5'-TCATTATCATCAATGCCACCCACGGAAAAATACAGGTG-3', the pDONR201-SLFN11 plasmid was used as a PCR template to add 4 tandem stop codons between the C-terminal end of SLFN11 cDNA and the Myc-DDK tag sequence to ensure

termination after the SLFN11 cDNA translation. Site-directed mutagenesis of mouse Twist1 cDNA to the DNA-binding mutant K145E (Maia et al., 2012) was performed using a QuikChange Site-Directed Mutagenesis Kit (Agilent) and the following primers: forward 5'-GGACAAGCTGAGCGAGATTCAAGACCC-3' and reverse 5'-GGGTCTGAATCTCGCTCAGCTTGTCC-3'. Gateway® cloning was performed according to manufacturer's recommendations (BP/LR clonase enzyme mixes; Life Technologies). The plasmid pLIX\_402 was a gift from David Root (Addgene plasmid #41394) and pLT3GEPIR (Fellmann et al., 2013) was obtained from the MSKCC RNAi core facility. A list of tested shRNA sequences is available in Table S3. Lentiviral supernatants were generated and titered in 293T/17 cells as previously described (Lok et al., 2016; Moffat et al., 2006). Briefly, a multiplicity of infection (MOI) of ~1 was used to infect target cells in the presence of 8 µg/mL hexadimethrine bromide (polybrene). For suspension cells, viral transductions were performed in a swinging bucket rotor at 37 °C for 30 min at 800 x g, before placing cells back into culture. One day later, media was changed on target cells. One day following media change, selection with puromycin proceeded daily for 5-7 d to establish stably transduced cell cultures. Cells transduced with doxycycline-sensitive elements were maintained in tetracycline-free media (Clontech) prior to induction. Sanger sequencing of plasmids was performed by Genewiz, Inc. Nucleotide and protein sequence alignments were performed in Geneious Pro 4.7.6.

#### shRNA sequences

Target	Species	Text ID	97mer sequence (5'-3')
<i>TWIST1</i>	Human	shTWIST1.1	TGCTGTTGACAGTGAGCGCCCTCGGACAAGCTGAGCAATAGTGAAGC CACAGATGTATTGCTCAGCTGTCCGAGGGCATGCCTACTGCCTCGGA
<i>TWIST1</i>	Human	shTWIST1.2	TGCTGTTGACAGTGAGCGACCAGGGCAAGCGCGCAAGAATAGTGAAG GCCACAGATGTATTCTGCCCGCTTGCCTGGGTGCCTACTGCCTCGGA A
Renilla luciferase	Sea Pansy	shRenilla	TGCTGTTGACAGTGAGCGCAGGAATTATAATGCTTATCTATAAGTGAAG CCACAGATGTATAGATAAGCATTATAATTCTATGCCTACTGCCTCGGA
<i>Twist1</i>	Mouse	shTwist1.1	TGCTGTTGACAGTGAGCGCCCTCGGACAAGCTGAGCAATAGTGAAG CCACAGATGTATTGCTCAGCTGTCCGAGGGCATGCCTACTGCCTCGGA
<i>Twist1</i>	Mouse	shTwist1.2	TGCTGTTGACAGTGAGCGAACAAAGCTGAGCAAGATTAGATAGTGAAG CCACAGATGTATCTGAATCTGCTCAGCTGTGCCTACTGCCTCGGA
<i>SLFN11</i>	Human	shSLFN11.1	TGCTGTTGACAGTGAGCGCCAGTTGTCTGAAGATTTGAATAGTGAAG CCACAGATGTATTCAAATCTCAGACAACTGTTGCCTACTGCCTCGGA
<i>SLFN11</i>	Human	shSLFN11.2	TGCTGTTGACAGTGAGCGATCAGTTCTCATTATAACGTATAGTGAAG CACAGATGTATACGGTATAATGAAGAACTGAGTGCCTACTGCCTCGGA
<i>EZH2</i>	Human	shEZH2.1	TGCTGTTGACAGTGAGCGAAAGAGGGAAAGTGTATGATAATAGTGAAG CCACAGATGTATTATCATACTTCCTCTGCCTACTGCCTCGGA
<i>EZH2</i>	Human	shEZH2.2	TGCTGTTGACAGTGAGCGCCGAAATTCCCTCTGATAAATAGTGAAG CCACAGATGTATTATCAGAAGGAAATTCCGATGCCTACTGCCTCGGA

#### In vivo irradiation

Once tumor volumes reached approximately 150 mm<sup>3</sup>, mice were randomized to control and treatment arms. Flank irradiation was administered at 2 Gy/fraction to anesthetized mice for 4 consecutive days delivered by an X-Ray irradiator (XRAD 320, Precision X-Ray) with secondary collimation by custom lead cut-outs.

#### DNA/RNA extraction and sequencing

DNA and RNA were extracted from flash frozen tissue using AllPrep DNA/RNA mini kits (Qiagen; 80204), homogenizing tissue using a gentleMACS M tube containing ~2 mL of RLT Plus buffer (Qiagen; 1053393) supplemented with 2-mercaptoethanol (Fisher) and processing samples on a pre-specified RNA extraction cycle. Samples were passed through QIAshredder columns (Qiagen; 79656) and DNA and RNA components were eluted in water before storing DNA at -20 °C and RNA at -80 °C for future analyses. RNA library preparation (w/ polyA selection), multiplexing and sequencing on an Illumina HiSeq2500 in RapidRun mode (50 bp single end reads) was performed by Genewiz. SureSelect Human All Exon V4 and SureSelect Mouse All Exon enrichment kits (Agilent) were used for whole exome library preparation. MSK-IMPACT (Cheng et al., 2015; Wagle et al., 2012) and whole exome sequencing on most samples was performed by the MSKCC integrated genomics operation (iGO) core facility. Additional whole exome sequencing was performed at Genewiz.

### Protein extraction, near-infrared Western blotting and protein quantitation

Whole cell lysates were prepared from frozen cell pellets or flash frozen tissue using radioimmunoprecipitation assay (RIPA) buffer lysis and extraction buffer (Thermo; 89901) supplemented with Halt™ protease and phosphatase inhibitor cocktail (Thermo; 78440). For extraction from frozen tissue, 50-100 mg of tissue was placed into gentleMACS M tube (Miltenyi; 130-094-392) in ~2 ml of ice-cold extraction buffer and processed using a pre-specified protein extraction cycle, followed by a 10 s sonication setup using 200V microtip sonicator set to 40% amplitude (QSonica; CL18). Crude lysates were clarified at 14,000 rpm for 10 min in a refrigerated bench top centrifuge (Eppendorf; 5340 R). Protein lysates were quantified using a micro BCA protein assay kit (Pierce; 23235) and then diluted with extraction buffer, NuPAGE® LDS sample buffer and reducing reagent (Life Technologies) prior to resolving on 4-12% Bis-Tris gradient gels. Gels were wet-transferred to 0.45 µm Immobilon-FL PVDF membrane (Millipore; IPFL00010, lot#R5GA0255H for all blots reported). All primary antibodies were incubated overnight with membranes in TBS Odyssey blocking buffer supplemented with 0.1% Tween-20 (LI-COR; 927-50000), while secondary antibodies were incubated at room temperature with agitation for 1 hr in primary blocking buffer supplemented with 0.01% SDS. Membranes were dried at 37 C and protected from light before imaging (LI-COR; Odyssey Sa). The same instrument gain settings were used for all targets examined (3.0 for 700 nm channel; 6.0 for 800 nm channel), with normalization of the 800 nm channel against the 700 nm channel, where indicated in the text or figure legend. Images were analyzed in ImageStudio (LI-COR; version 3.1.4) Recombinant GST-SLFN11 (Abnova; H00091607-P01) was used to determine the limit of detection for SLFN11 in cell lines and PDX tissue. 5 µg of total, clarified cell lysate was determined to be optimal for detection of 4 logs of dynamic range of for SLFN11 from in vivo sources.

### Antibodies

Target	Source	Product#	Application	Fold Dilution
EZH2	Cell Signaling	5246	WB	1000
EZH2	Active Motif	39901	ChIP	5ug/reaction
H3K27me1	Active Motif	61015	WB	1000
H3K27me2	Cell Signaling	9728	WB	2500
H3K27me3	Active Motif	39155	WB	2500
H3K27me3	Millipore	07-449	ChIP	4ug/reaction
H3K36me3	Cell Signaling	4909	WB	1000
H3K4me3	Cell Signaling	9751	WB	1000
H3K27Ac	Active Motif	39685	WB	1000
H3K27Ac	Active Motif	39133	ChIP	4ug/reaction
actin (mouse)	Cell Signaling	3700	WB	5000
actin (rabbit)	Cell Signaling	8457	WB	5000
H3 (mouse)	Cell Signaling	14269	WB	5000
H3 (rabbit)	Cell Signaling	4499	WB	5000
vinculin	Cell Signaling	13901	WB	1000
TWIST1	Abcam	ab50887	WB	1000
SLFN11	Santa Cruz	sc-374339	WB	250
cleaved-PARP	Cell Signaling	5625	WB	1000
γH2A.X (phospho-S139)	Cell Signaling	9718	WB	1000
H2A.X	Cell Signaling	2595	WB	1000
GFP	Cell Signaling	2956	WB	5000
donkey anti-rabbit IRDye 800CW	LI-COR	926-32213	WB	25000
donkey anti-mouse IRDye 680LT	LI-COR	926-68022	WB	25000
donkey anti-mouse IRDye 800CW	LI-COR	926-32212	WB	25000
donkey anti-rabbit IRDye 680LT	LI-COR	926-68023	WB	25000
SLFN11	Santa Cruz	sc-374339	IHC	2ug/mL
Chromogranin A	Ventana	LK2H10	IHC	2000
Synaptophysin	BIOGENEX	Snp88	IHC	2000
Ki67/MIB1	DAKO	M7240	IHC	200

### Mutation and copy number analysis

Raw reads were aligned to a custom hybrid reference genome using BWA 0.7.12-r1039 with default settings (Li and Durbin, 2009). The hybrid index was generated using a FASTA file consisting of all human GRCh38 and mouse GRCm38.p3 reference contigs as previously described (Schneeberger et al., 2016). Mapped reads were piped to SAMBLASTER 0.1.22 and samtools 1.2 for on-the-fly duplicate removal and sorting, respectively. Sorted reads were processed through the Genome Analysis Toolkit (GATK) 3.6, according to standard practices, including generation of depth of coverage analysis statistics (DePristo et al., 2011; McKenna et al., 2010). Each sample was genotyped at >1,000 common SNP sites using HaplotypeCaller to generate a fingerprint. SNP concordance was confirmed by bcftools 1.2. Mutations and indels were called using MuTect2 and annotated with the subset of common SNPs in dbSNP 147 found in >1% of the population. Variants that did not pass a MuTect2 filter, had a variant frequency <10%, or were a common SNP were excluded. Filtered mutations were annotated with snpEff (Cingolani et al., 2012). Final mutations and their annotations were loaded into the R statistical computing environment for final analysis. For novel mutation discovery, genes were

rank ordered by the number of models in which a gene was mutated in the chemoresistant setting, but not the chemonaive setting. Mutational signature data was generated by deconstructSigs v1.8.0 (Rosenthal et al., 2016). Copy number data was generated using FACETS v0.3.30 (Shen and Seshan, 2016). Copy number plots were generated using the copynumber package for R (Nilsen et al., 2012).

### Gene expression analysis

Raw reads were aligned to a custom hybrid reference genome using STAR 2.4.1b (Dobin et al., 2013). The hybrid index was generated using a FASTA file consisting of all human GRCh38 and mouse GRCm38.p3 reference contigs and the human GENCODE gene set release 20 transcript model as previously described (Schneeberger et al., 2016). Mapped reads were assigned to GENCODE 20 genes using Subread 1.5.0-p2 to generate a raw counts table (Liao et al., 2014). Raw counts were read into the R statistical computing environment for further analysis (R Core Team (2016). R: A language and environment for statistical computing. R Foundation for Statistical Computing, Vienna, Austria. URL: <https://www.R-project.org/>). Downstream analysis was performed with the limma package for R (Ritchie et al., 2015). Genes with  $\geq 5$  counts per million in  $\geq 3$  samples were considered for analysis. Counts were normalized to library size and transformed to log2 counts per million with upper quartile normalization. Weights were calculated based on a combination of observational-level weights determined from an estimate of the mean-variance relationship within all samples and sample-level weights reflecting the degree to which each sample follows the linear model (Ritchie et al., 2006). A linear model was fit for each contrast and standard errors were moderated using an empirical Bayes method. T statistics, B statistics, and p values were generated for each gene. P values were corrected for multiple testing by the method of Bonferroni. To identify genes with biologically significant effect sizes, statistically significant p values, and recurrent alterations, we chose to highlight genes with a fold change of  $\geq 1.5$  that were significant in  $\geq 3$  models.

Robust Multi-array Average (RMA) and quantile normalized gene expression microarray data for 1,037 cancer cell lines was downloaded from the Cancer Cell Line Encyclopedia (Barretina et al., 2012). The gene expression signal distribution of *SLFN11* is distinctly bimodal. The minor mode comprises cell lines in which the gene is not expressed while the major mode, having a greater standard deviation, comprises cell lines in which *SLFN11* is expressed at varying levels. To discriminate between cell lines based on *SLFN11* expression, a gene expression cutoff was established using two independent approaches: the method of Zilliox et al. (Zilliox and Irizarry, 2007), which estimates a gene expression cutoff based on the standard deviation of the minor mode based on the left side of the mean, and by fitting a finite mixture of 2 Gaussian components. Both approaches were in agreement in establishing a cutoff of 5.

### ChIP-seq and ChIP-qPCR

Tumor tissue was submersed 1% formaldehyde in PBS, cut into small pieces and incubated at room temperature for 15 min. Fixation was stopped by the addition of 0.125 M glycine (final concentration). The tissue pieces were then treated with a TissueTearer and finally spun down and washed twice in PBS. Chromatin was isolated by the addition of lysis buffer, followed by disruption with a Dounce homogenizer. NCI-H446 cells were fixed with 1% formaldehyde for 15 min and quenched with 0.125 M glycine. Chromatin was isolated by the addition of lysis buffer, followed by disruption with a Dounce homogenizer. Lysates were sonicated and the DNA sheared to an average length of 300-500 bp. Genomic DNA (Input) was prepared by treating aliquots of chromatin with RNase, proteinase K and heat for de-crosslinking, followed by ethanol precipitation. Pellets were re-suspended and the resulting DNA was quantified on a NanoDrop spectrophotometer. Extrapolation to the original chromatin volume allowed quantitation of the total chromatin yield. Aliquots of chromatin (20-30  $\mu$ g) were pre-cleared with protein A agarose beads (Invitrogen). Genomic DNA regions of interest were isolated using 5  $\mu$ l antibody against EZH2 (Active Motif; 39901), or 4  $\mu$ g of antibody against H3K27Ac (Active Motif; 39133) and H3K27me3 (Millipore; 07-449). Complexes were washed, eluted from the beads with SDS buffer, and subjected to RNase and proteinase K treatment. Crosslinks were reversed by incubation overnight at 65 C, and ChIP DNA was purified by phenol-chloroform extraction and ethanol precipitation. Quantitative PCR (qPCR) reactions were carried out by Active Motif in triplicate using SYBR Green Supermix (Bio-Rad; 170-8882) on a CFX Connect<sup>TM</sup> Real Time PCR system. The *SLFN11* primer pair targeting upstream of the first exon are as follows: forward 5'-CGAGCCAGAGTGGGATTTAAC-3' and reverse 5'-TTTCATATCACTAGCAGCGTGAC-3'. The resulting signals were normalized for primer efficiency by carrying out qPCR for each primer pair using Input DNA (pooled unprecipitated DNA from cells or tissues). Test sites were run alongside the positive control sites targeted to the *ACTB* promoter (Active Motif; 71023) and *CCND2* gene (Active Motif; 71008) and a negative control primer pair that amplifies a region in a gene desert on chromosome 12 (Active Motif; 71001). For *SLFN11* exon-by-exon ChIP-qPCR, the following primers were used: exon 1 forward 5'-CACGGGTAGAACGCAACTC-3' and reverse 5'-GCTGGAGCTTGAGAGGTGAC-3', exon 2 forward 5'-GAAACAAAAGCACCTGATTCTAGTC-3' and reverse 5'-TTGGTGGGAACTCTGGCTAC-3', exon 3 forward 5'-TTCTTACCAACCTTGCCTAGTTAG-3' and reverse 5'-TGGTCTTGAATGCAGAATG-3', exon 4 forward 5'-TTGGCTTCCTTTGGTCTTC-3' and reverse 5'-CTTGCAGCCTCAGTTCTTC-3', exon 5 forward 5'-GCAGAGCACTTCAGGATTTAC-3' and reverse 5'-TCTCAACACCAGCCAGTTTC-3', exon 6 5'-CAAAATCCCCGAAAGAAAG-3' and reverse 5'-CTCTGGAGGGACCTGATCTC-3', and exon 7 5'-TCATTTCATCTTGGCCTATAATTTC-3' and reverse 5'-TGGTCTCCAGAGCTTGTCTC-3'. Data are reported as "binding events per 1000 cells" which considers chromatin input, ChIP volumes and primer pair efficiencies. Illumina sequencing libraries were prepared from the ChIP and Input DNAs by the standard consecutive enzymatic steps of end-polishing, dA-addition, and adaptor ligation. After a final PCR amplification step, the resulting DNA libraries were quantified and sequenced on Illumina's NextSeq 500 (75 bp single ended reads). Reads were aligned to the human

genome (hg19) using BWA (Li and Durbin, 2009) algorithm (default settings). Duplicate reads were removed and only uniquely mapped reads (mapping quality  $\geq 25$ ) were used for further analysis. Alignments were extended in silico at their 3'-ends to a length of 200 bp, which is the average genomic fragment length in the size-selected library, and assigned to 32 bp bins along the genome. The resulting histograms (genomic “signal maps”) were stored in bigWig files. ChIP target enriched regions were identified using the SICER (Zang et al., 2009) algorithm (FDR  $1E^{-10}$ , gap = 600 bp). Drosophila genome spike-in was used to downsample and normalize tag counts for comparisons across treated and untreated samples (Active Motif; ChIP Normalization Strategy) (Orlando et al., 2014). For the spike-in adjusted analysis, the downscaling of H3K27me3 in the EPZ-treated samples was  $>5$ -fold, compared to the vehicle controls. In addition, the resistant vehicle H3K27Ac data was downscaled by  $\sim 2.5$ -fold as compared to all other samples. The EZH2 data was only normalized by  $<1.5$ -fold across all samples based on the spike-in tag counts. All plots were generated using the R statistical computing environment.

## SUPPLEMENTAL REFERENCES

- Campbell, J. E., Kuntz, K. W., Knutson, S. K., Warholic, N. M., Keilhack, H., Wigle, T. J., Raimondi, A., Klaus, C. R., Rioux, N., Yokoi, A., *et al.* (2015). EPZ011989, A Potent, Orally-Available EZH2 Inhibitor with Robust in Vivo Activity. *ACS Med Chem Lett* 6, 491-495.
- Cheng, D. T., Mitchell, T. N., Zehir, A., Shah, R. H., Benayed, R., Syed, A., Chandramohan, R., Liu, Z. Y., Won, H. H., Scott, S. N., *et al.* (2015). Memorial Sloan Kettering-Integrated Mutation Profiling of Actionable Cancer Targets (MSK-IMPACT): A Hybridization Capture-Based Next-Generation Sequencing Clinical Assay for Solid Tumor Molecular Oncology. *J Mol Diagn* 17, 251-264.
- Cingolani, P., Platts, A., Wang le, L., Coon, M., Nguyen, T., Wang, L., Land, S. J., Lu, X., and Ruden, D. M. (2012). A program for annotating and predicting the effects of single nucleotide polymorphisms, SnpEff: SNPs in the genome of *Drosophila melanogaster* strain w1118; iso-2; iso-3. *Fly (Austin)* 6, 80-92.
- DePristo, M. A., Banks, E., Poplin, R., Garimella, K. V., Maguire, J. R., Hartl, C., Philippakis, A. A., del Angel, G., Rivas, M. A., Hanna, M., *et al.* (2011). A framework for variation discovery and genotyping using next-generation DNA sequencing data. *Nat Genet* 43, 491-498.
- Dobin, A., Davis, C. A., Schlesinger, F., Drenkow, J., Zaleski, C., Jha, S., Batut, P., Chaisson, M., and Gingeras, T. R. (2013). STAR: ultrafast universal RNA-seq aligner. *Bioinformatics* 29, 15-21.
- Fellmann, C., Hoffmann, T., Sridhar, V., Hopfgartner, B., Muhar, M., Roth, M., Lai, D. Y., Barbosa, I. A., Kwon, J. S., Guan, Y., *et al.* (2013). An optimized microRNA backbone for effective single-copy RNAi. *Cell Rep* 5, 1704-1713.
- Hann, C. L., Daniel, V. C., Sugar, E. A., Dobromilskaya, I., Murphy, S. C., Cope, L., Lin, X., Hierman, J. S., Wilburn, D. L., Watkins, D. N., and Rudin, C. M. (2008). Therapeutic efficacy of ABT-737, a selective inhibitor of BCL-2, in small cell lung cancer. *Cancer Res* 68, 2321-2328.
- Jahchan, N. S., Dudley, J. T., Mazur, P. K., Flores, N., Yang, D., Palmerton, A., Zmoos, A. F., Vaka, D., Tran, K. Q., Zhou, M., *et al.* (2013). A drug repositioning approach identifies tricyclic antidepressants as inhibitors of small cell lung cancer and other neuroendocrine tumors. *Cancer Discov* 3, 1364-1377.
- Kononen, J., Bubendorf, L., Kallioniemi, A., Barlund, M., Schraml, P., Leighton, S., Torhorst, J., Mihatsch, M. J., Sauter, G., and Kallioniemi, O. P. (1998). Tissue microarrays for high-throughput molecular profiling of tumor specimens. *Nat Med* 4, 844-847.
- Leong, T. L., Marini, K. D., Rossello, F. J., Jayasekara, S. N., Russell, P. A., Prodanovic, Z., Kumar, B., Ganju, V., Alamgeer, M., Irving, L. B., *et al.* (2014). Genomic characterisation of small cell lung cancer patient-derived xenografts generated from endobronchial ultrasound-guided transbronchial needle aspiration specimens. *PLoS One* 9, e106862.
- Li, H., and Durbin, R. (2009). Fast and accurate short read alignment with Burrows-Wheeler transform. *Bioinformatics* 25, 1754-1760.
- Liao, Y., Smyth, G. K., and Shi, W. (2014). featureCounts: an efficient general purpose program for assigning sequence reads to genomic features. *Bioinformatics* 30, 923-930.
- Lok, B. H., Gardner, E. E., Schneeberger, V. E., Ni, A., Desmeules, P., Rekhtman, N., de Stanchina, E., Teicher, B. A., Riaz, N., Powell, S. N., *et al.* (2016). PARP Inhibitor Activity Correlates with SLFN11 Expression and Demonstrates Synergy with Temozolomide in Small Cell Lung Cancer. *Clin Cancer Res*.
- McKenna, A., Hanna, M., Banks, E., Sivachenko, A., Cibulskis, K., Kernytsky, A., Garimella, K., Altshuler, D., Gabriel, S., Daly, M., and DePristo, M. A. (2010). The Genome Analysis Toolkit: a MapReduce framework for analyzing next-generation DNA sequencing data. *Genome Res* 20, 1297-1303.
- Moffat, J., Grueneberg, D. A., Yang, X., Kim, S. Y., Kloepfer, A. M., Hinkle, G., Piqani, B., Eisenhaure, T. M., Luo, B., Grenier, J. K., *et al.* (2006). A lentiviral RNAi library for human and mouse genes applied to an arrayed viral high-content screen. *Cell* 124, 1283-1298.
- Nilsen, G., Liestol, K., Van Loo, P., Moen Vollan, H. K., Eide, M. B., Rueda, O. M., Chin, S. F., Russell, R., Baumbusch, L. O., Caldas, C., *et al.* (2012). Copynumber: Efficient algorithms for single- and multi-track copy number segmentation. *BMC Genomics* 13, 591.

- Ocak, S., Yamashita, H., Udyavar, A. R., Miller, A. N., Gonzalez, A. L., Zou, Y., Jiang, A., Yi, Y., Shyr, Y., Estrada, L., *et al.* (2010). DNA copy number aberrations in small-cell lung cancer reveal activation of the focal adhesion pathway. *Oncogene* 29, 6331-6342.
- Orlando, D. A., Chen, M. W., Brown, V. E., Solanki, S., Choi, Y. J., Olson, E. R., Fritz, C. C., Bradner, J. E., and Guenther, M. G. (2014). Quantitative ChIP-Seq normalization reveals global modulation of the epigenome. *Cell Rep* 9, 1163-1170.
- Poirier, J. T., Dobromilskaya, I., Moriarty, W. F., Peacock, C. D., Hann, C. L., and Rudin, C. M. (2013). Selective tropism of Seneca Valley virus for variant subtype small cell lung cancer. *J Natl Cancer Inst* 105, 1059-1065.
- Ritchie, M. E., Diyagama, D., Neilson, J., van Laar, R., Dobrovic, A., Holloway, A., and Smyth, G. K. (2006). Empirical array quality weights in the analysis of microarray data. *BMC Bioinformatics* 7, 261.
- Ritchie, M. E., Phipson, B., Wu, D., Hu, Y., Law, C. W., Shi, W., and Smyth, G. K. (2015). limma powers differential expression analyses for RNA-sequencing and microarray studies. *Nucleic Acids Res* 43, e47.
- Rosenthal, R., McGranahan, N., Herrero, J., Taylor, B. S., and Swanton, C. (2016). DeconstructSigs: delineating mutational processes in single tumors distinguishes DNA repair deficiencies and patterns of carcinoma evolution. *Genome Biol* 17, 31.
- Saunders, L. R., Bankovich, A. J., Anderson, W. C., Aujay, M. A., Bheddah, S., Black, K., Desai, R., Escarpe, P. A., Hampl, J., Laysang, A., *et al.* (2015). A DLL3-targeted antibody-drug conjugate eradicates high-grade pulmonary neuroendocrine tumor-initiating cells in vivo. *Sci Transl Med* 7, 302ra136.
- Shen, R., and Seshan, V. E. (2016). FACETS: allele-specific copy number and clonal heterogeneity analysis tool for high-throughput DNA sequencing. *Nucleic Acids Res* 44, e131.
- Wagle, N., Berger, M. F., Davis, M. J., Blumenstiel, B., Defelice, M., Pochanard, P., Ducar, M., Van Hummelen, P., Macconnaill, L. E., Hahn, W. C., *et al.* (2012). High-throughput detection of actionable genomic alterations in clinical tumor samples by targeted, massively parallel sequencing. *Cancer Discov* 2, 82-93.
- Zang, C., Schones, D. E., Zeng, C., Cui, K., Zhao, K., and Peng, W. (2009). A clustering approach for identification of enriched domains from histone modification ChIP-Seq data. *Bioinformatics* 25, 1952-1958.
- Zilliox, M. J., and Irizarry, R. A. (2007). A gene expression bar code for microarray data. *Nat Methods* 4, 911-913.